MECHANICAL PROPERTIES OF ADDITIVELY MANUFACTURED STAINLESS STEEL

THESIS

Eric W. Lum, Capt, USAF

AFIT-ENY-MS-17-M-273

DEPARTMENT OF THE AIR FORCE
AIR UNIVERSITY

AIR FORCE INSTITUTE OF TECHNOLOGY

Wright-Patterson Air Force Base, Ohio

DISTRIBUTION STATEMENT A
APPROVED FOR PUBLIC RELEASE; DISTRIBUTION UNLIMITED.

The views expressed in this document are those of the author and do not reflect the official policy or position of the United States Air Force, the United States Department of Defense or the United States Government. This material is declared a work of the U.S. Government and is not subject to copyright protection in the United States.

AFIT-ENY-MS-17-M-273

MECHANICAL PROPERTIES OF ADDITIVELY MANUFACTURED STAINLESS STEEL

THESIS

Presented to the Faculty

Department of Aeronautical Engineering

Graduate School of Engineering and Management

Air Force Institute of Technology

Air University

Air Education and Training Command

in Partial Fulfillment of the Requirements for the

Degree of Master of Science in Aeronautical Engineering

Eric W. Lum, B.S.M.E.

Capt, USAF

March 3, 2017

DISTRIBUTION STATEMENT A
APPROVED FOR PUBLIC RELEASE; DISTRIBUTION UNLIMITED.

AFIT-ENY-MS-17-M-273

MECHANICAL PROPERTIES OF ADDITIVELY MANUFACTURED STAINLESS STEEL

Eric W. Lum, B.S.M.E.
Capt, USAF

Committee Membership:

Dr. Anthony Palazotto, PhD
Chair

Dr. Philip Flater Abrahams, PhD
Member

Dr. Marina Ruggles-Wrenn, PhD
Member

Abstract

The Air Force (AF) is interested in exploring how additive manufacturing (AM) may benefit the design and construction of aerospace structures. The AM process is capable of easily creating parts that are difficult to machine using traditionally wrought materials. This process can significantly reduce the amount of waste material and shorten the logistics time to receive a new part. In order to use AM materials the AF must first understand how the AM process affects the material properties. The material that will be analyzed is 15-5PH stainless steel which is commonly used in the aerospace industry. The research will analyze two different build orientations as well as two different heat treatments, Condition A and H900. There are multiple techniques that can be used create parts through AM such as extrusion deposition, metal wire processing, powder fed directed energy deposition and powder bed fusion. This research will focus on the powder bed fusion, using the Direct Metal Laser Sintering technique which is often used with 15-5PH stainless steel. In order to understand how the material properties are effected by the AM process, research is being conducted using quasi-static and Split Hopkinson Pressure Bar testing to evaluate the mechanical properties of 15-5PH stainless steel. This on-going research will extend the previous analysis of tension loading at high strain rates analysis to compression loading at high strain rates. Electron backscatter diffraction (EBSD) will be used to analyze the microstructure of specimens to analyze the affect that the DMLS process has on the microstructure. The results of the compression testing will be compared to the results from the tension testing to compare the mechanical response to the two different load types.

Acknowledgments

I would like to thank several people for the help that they have given me on this project. Maj Allison Dempsey who first introduced me to this subject and allowed me to shadow her while she was conducting her research. She showed me how to start my research and gave me invaluable advice on how to conduct it. I would also like to thank my committee members Dr. Palazotto, Committee Chairman, Dr. Flatter and Dr. Ruggles-Wren for their valued technical advice and support. I would like to thank my sponsor Mr. Don Littrell from AFRL/RW for his support of additive manufacturing research and specifically for supporting this research effort. I want to thank Dr. Flatter and Mr. Harris from AFRL/RW for all of the support they gave me conducting my testing, helping me with my micro structural analysis and interpreting the results of my data. I would also like to thank Professor Nie from Southern Methodist University for the use of his Split Hopkinson Bar for conducting my tests.

Eric W. Lum

Table of Contents

Page

List of Figures

List of Tables

List of Acronyms

M_F	Martensite Finish
M_S	Martensite Start
AF	Air Force
AISI	American Iron and Steel Institute
AM	Additive Manufacturing
BCC	Body Centered Cubic
CAD	Computer Aided Design
DIC	Digital Image Correlation
DMLS	Direct Metal Laser Sintering
EBSD	Electron Backscatter Diffraction
EDS	Energy Dispersive X-ray Spectroscopy
EOS	Electro Optical Systems
FCC	Face Centered Cubic
FS	Failure Strain
PBF	Powder Bed Fusion
PH	Precipitation Hardening
SEM	Scanning Electron Microscope
SHPB	Split Hopkinson Pressure Bar
UNS	Unified Numbering System
UTS	Ultimate Tensile Strength
YS	Yield Strength

List of Symbols

ϵ	Strain
ϵ_I	Incident Strain
ϵ_R	Reflected Strain
ϵ_T	Transmission Strain
σ_{AVG}	Average Stress
C_{BAR}	Elastic Wave Speed in the Incident and Transmission Bar
C_{st}	Elastic Wave Speed in the Striker Bar
D_{BAR}	Incident and Transmission Bar Diameter
D_S	Specimen Diameter
E_{BAR}	Young's Modulus of the Incident and Transmission Bar
F_1	Force at Interface 1
F_2	Force at Interface 2
F_{AVG}	Average Force
L_{st}	Length of Striker Bar
L_S	Length of Specimen
v_1	Particle Velocity at Interface 1
v_2	Particle Velocity at Interface 2
E	Young's Modulus
T	Duration of Loading
u	Axial Displacement
v	Particle Velocity

MECHANICAL PROPERTIES OF ADDITIVELY MANUFACTURED STAINLESS STEEL

I. Introduction

1.1 Background

Additive Manufacturing (AM) has steadily evolved over the last couple of decades from an industry that was primarily used to create models of complex shapes into an industry that creates parts undergoing heavy loads. As the industry continues to grow and expand we will begin to see AM parts start to integrate into the modern product production line. The current technology is starting to make its way into the market, but is relatively limited due to the high costs of a developing technology and the need for further research into understanding the effects that the process has on the material being produced.

The AM process is a highly complex process which integrates cutting edge technology of multiple disciplines into a single process to produce the part. This marriage of mechanical engineering, materials engineering and optics has resulted in an ability to create parts that could only be dreamed about using traditional manufacturing methods. Traditional manufacturing methods require the ability to either remove material from the part or remove the mold the part is created in. These methods severely limit the geometry that can be produced. Because the process of AM builds the part up, it does not have those same limitations and is able to create significantly more complex geometries.

The other advantage of the AM process is its ability to quickly and easily create

customized parts. With traditional manufacturing, it is often expensive and difficult to create custom parts. After a production line has shut down, it is extremely difficult to find replacement parts, but through AM a simple scan of the part can be conducted to get the parts dimensions, and then a new one can be printed. This ability is becoming extremely popular in the medical field. Custom dental implants that exactly match the original tooth can be printed. Replacement hips and joints can be created to the exact specifications of the original making it much easier for the new prosthetic part to integrate with the body.

These advantages also crossover to the automotive and aerospace industry. AM allows for the creation of internal channels in solid pieces that can allow a coolant to flow through. This allows for the cooling of turbine blades in turbine engines. By being able to better cool the turbine blades, the temperature of the engine can be increased, increasing both the power and efficiency of the engine. The AM process is also able to create complex internal lattice and truss structures for parts that proved high strength at a reduced weight.

There are several key advantages to the AM process, the first of which is how highly automated the process is. Once a Computer Aided Design (CAD) file of the desired part is sent to the machine, it is able to read the part and create the production process on its own. Once the machine begins production, it can be left alone until the parts are finished. This process requires very little manpower, and can be left to operate overnight, and over weekends increasing production.An additional advantage of AM is the reduction of turnaround between parts. After one part is completed, a new CAD file can be uploaded and production of a new part started immediately. Another advantage to the AM process is that is builds the part up from nothing instead of removing material. The buildup process results in very little waste material especially when compared to the subtractive methods of traditional

manufacturing. This also requires significantly less stock material to create a part. These advantages result in a lower cost to produce a part. The reduction in cost, and the advantages provided by the ability to create these new complex geometries must also be weighed against some of the known disadvantages.

During the development of the AM process, there were several disadvantages that were discovered. As the AM process produces the part by adding layers of material together to create the part, each layer of the part is exposed to the atmosphere. This process can expose the internal material to humidity. This exposure may result in oxidization and corrosion issues. During the build process the machine atmosphere is controlled, typically argon or nitrogen, to prevent ignition of the powder. The build atmosphere may also have an effect on the chemistry of the alloy. Another disadvantage is the buildup of internal stresses that form as a result of temperature differences across the part. These internal stresses can be relieved through a stress relieving heat treatment, but that typically reduces the mechanical properties. Another disadvantage of the AM, process is the resulting surface roughness of the part. When the part comes out of the machine, the surface of the part is usually very rough. The increased surface roughness of AM parts typically result in a reduction of the life cycle of the part.

The advantages that the AM process has are something the Air Force (AF) is really interested in. The AF typically procures systems that are not typically of interest to the general public. This results in a relatively small number of systems being built, which results in increased costs per part due to the cost of the specialized tooling to create the part. The AF also has numerous systems that have aged to the point that there is no longer a production line. Through the use of AM replacement parts would be significantly cheaper to build and could be produced at any time. However, in order to approve parts created through this new process, they need to

fully characterize the material properties and asses how the AM process effects the material.

1.2 Research Scope

The objective of this research is to establish the mechanical properties of AM 15-5PH stainless steel. In order to be able to characterize any effect the new manufacturing method may have on the material, there were several parameters selected that would be varied in order to see if they were effected. This research identified three variables that would be examined: build orientation, heat treatment, and strain rate. Build orientation was selected to establish whether the AM process and the orientation that the part is built in has an effect on the material. The effect of the build orientation will determine if the material is isotropic, or anisotropic. Heat treatment was selected to verify that the material still reacts to heat treatment in the same manner that traditional wrought materials due. Heat treatment was also selected to see if any anisotropy of the material is enhanced during the heat treatment, or potentially reduced. The final variable selected was strain rate. This research is being conducted to support an effort by the AF to build a weapon through AM. Quasi Static data can be used for the material properties of the weapon through the majority of its life, but when the weapon is finally used, the forces on it will not be quasi static, but dynamic. In order to understand how the material reacts during these dynamic events the mechanical properties need to be established under a dynamic load.

This study desires to characterize the mechanical properties of the material, in order to do that we wish to reduce any impact that defects in the material may have. In order to reduce the potential impact of internal defects from the AM, process the parts will be produced using the manufactures recommended settings. These settings are well studied by the manufacturer to minimize the potential of internal

defects caused by partially sintered powder or excessive laser energy. Because the AM process often results in increased surface roughness, the specimens to be tested will be machined from larger AM samples. The machining will also eliminate any potential edge cracks that can form due to the temperature gradients across the part.

II. Background

Chapter two provides the background information on the material that is being tested as well as the theory behind the test methods. The material properties and composition of 15-5PH stainless steel as well as the theory behind the heat treatment will be reviewed. This chapter will discuss the Additive Manufacturing (AM) technique that was used to create the test specimens and the strengths and weakness of it. The theory behind the quasi-static and Split Hopkinson Pressure Bar (SHPB) mechanical tests will be discussed along with the optical microsopy, Electron Backscatter Diffraction (EBSD), and Energy Dispersive X-ray Spectroscopy (EDS) material property tests.

2.1 15-5 Precipitation Hardening Stainless Steel

2.1.1 15-5 Precipitation Hardening Stainless Steel Composition

15-5 PH Stainless steel is a martensitic Precipitation Hardening (PH) stainless steel that is ideally suited for the aerospace industry due to its strength, ductility and corrosion resistant properties. 15-5 PH is also often referred to as S15500 which is its designation by the Unified Numbering System (UNS). Martensitic stainless steels are iron alloys that are corrosion resistant and hardenable by heat treatment that allows them to be used in a variety of applications. The composition of 15-5PH is shown in Table 2.1

Element	Weight Percent (%)
C	0.07 max
Mn	1.00 max
Si	1.00 max
Cr	14.00-15.50
Ni	3.50-5.50
Mo	0.50 max
Nb	0.15-0.45
Cu	2.50-4.50
Fe	71.90-77.70 Balance

Table 2.1. AISI 15-5 PH Composition in %

All steels are primarily made of Fe which is relatively inexpensive and can provide high strength. Alloying elements are added in specific ratios for additional benefits, such as chromium which is added to increase the corrosion resistance of the steel. The chromium combines with oxygen to create a scale that covers the steel and prevents the iron corrosion as well as helping to stabilize the desired martensitic phase. Nickel is added to increase the toughness of the alloy and to help with corrosion resistance. Copper is added for the precipitation hardening effect that it has upon heat treatment. Manganese is used to combine with any sulfur that is in the alloy. Sulfur is a naturally occurring impurity that is often found in steel, when it combines with the iron it forms iron sulfides that increases the brittleness of the steel. The Manganese is added to prevent the formation of the iron sulfides by creating manganese sulfides that occur evenly throughout the grains, thus increasing the strength. Silicon is used in small amounts as a de-oxidizer and to promote the martensite/ferrite phases, but care should be taken as large quantities of silicon can increase the brittleness. Molybendum is added as a martensite/ferrite promoter, it can also pair up with the chromium to increase corrosion resistance. Carbon is one of the major promoters of strength and hardness in the steel when properly added. Excessive amounts of carbon can form undesirable carbides at the grain boundaries that weaken the steel.

Niobium is added to prevent those undesirable carbides from forming by forming its own beneficial carbides[2].

2.1.2 15-5 PH Stainless Steel Crystal Structure

15-5 PH stainless steel is designed to be a martensitic stainless steel, and in order to achieve the martensitic phase the steel is heated to transform its phase from the Body Centered Cubic (BCC) crystalline structure of ferrite to the Face Centered Cubic (FCC) phase of austenite shown in figure 2.1. The FCC crystal structure of austenite has significantly more space between the iron atoms of the BCC structure as shown. This increased space allows more of the alloying elements, such as carbon, to dissolve into the crystal structure than BCC structure of ferrite[3]. When the steel is cooled, the austenite will attempt to transform back into ferrite, and the carbon dissolved in the FCC structure of the austenite will diffuse to from cementite. However, if the steel is properly alloyed it will start to form martensite before forming ferrite. The Martensite Start (M_S) temperature is controlled by the alloying elements and can be adjusted as needed. When the steel reaches the Martensite Finish (M_F) temperature the austenite has completely changed to martensite. By increasing the M_S temperature higher, as the steel cools it will reach this temperatures faster allowing the martensite to form before any other phase will from. By increasing M_F temperature the austenite will completely transform to martensite faster, making the steel fully martensitic. As the crystal structure attempts to transform back into BCC it forms the highly strained body centered tetragonal (BCT) crystal of martensite[3] shown in figure 2.1. Shear deformations from as a result of the dislocations caused by the dissolved alloying elements. These dislocations strengthen of the steel. Without additional heat treatment 15-5 PH exhibits relatively good strength and ductility performance, but through additional heat treatment the strength can

be increased significantly. Upon air quenching 15-5PH has good strength and ductility performance, but is typically below that recommended for use. It is, however, easily machinable which makes it ideal for machining parts at low hardness, then heat treating to increase its strength to the desired level[4].

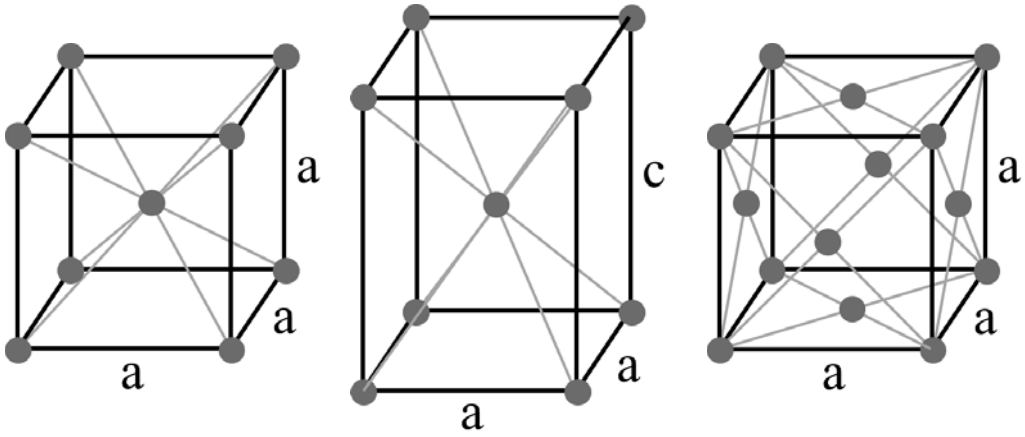

(a) BCC **(b) BCT** **(c) FCC**

Figure 2.1. 5-5 PH Stainless Steel Crystal Structure

2.1.3 15-5 Precipitation Hardening Stainless Steel Microstructure

15-5 PH Stainless steel is a fully lath martensitic structure. During the quenching process as the austenite grains cool they transform into martensite. The relatively low carbon content of 15-15 PH results in the formation of lath martensite. The crystals of lath martensite are shaped as thin plates of the same, or similar orientation adjacent to each other that form laths. The substructure of lath martensite contains a high density of dislocations which is similar to that of a metal subjected to strong cold deformation[5]. Martensite forms within the previous austenite grains and forms into packets that are then defined by blocks. Within each block forms the smaller lath substructure [6]. Figure 2.2 shows the lath martensite substructure that forms.

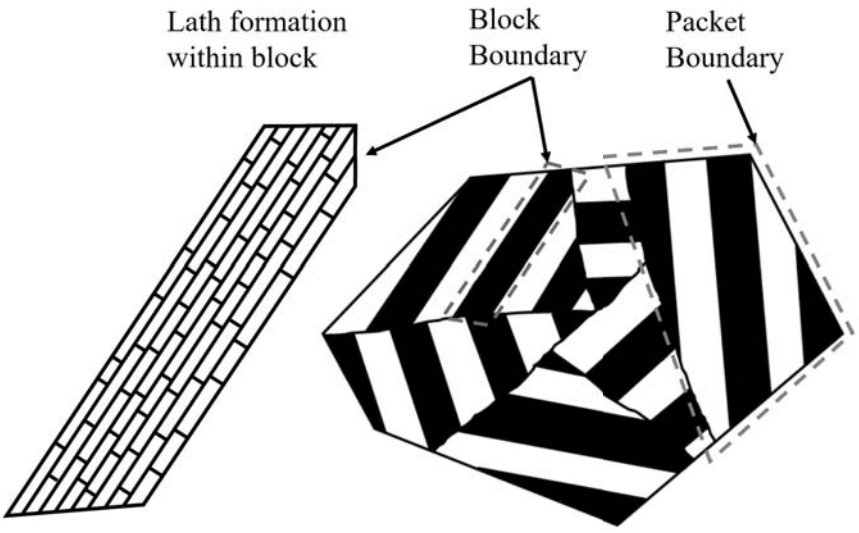

Figure 2.2. Microstructure of Martensite

2.1.4 15-5 Precipitation Hardening Stainless Steel Heat Treatment

When the steel is quenched, the 4% Cu becomes trapped in the BCT structure, over-saturating it. This over-saturation can be relieved by heating the steel to an intermediate temperature that allows the Cu to precipitate. This heat treatment is often referred to as precipitation hardening. Precipitation hardening relies on increasing the temperature of the steel enough that it allows the alloys trapped inside the BCT structure to diffuse and produce fine particles approximately 5 nm in diameter [7]. When these particles form inside a crystal structure, it results in a dislocation of the crystal lattice. These dislocations result in an increase of the strength of the steel[8]. For 15-5PH, the heat treatment temperature ranges from 900 to 1150 °F. In order to achieve the maximum strength of the steel by heat treatment, the 900 °F temperature is used to fully age the material. Heat treatment at higher temperatures such as 1050 or °F and 1150 °F result in decreased strength, but increased ductility and toughness and are referred to as overaged. The three heat treatments for S15500 defined by the American Iron and Steel Institute (AISI) are the H900, H1025 and H1150[9].

2.2 Direct Metal Laser Sintering

AM is a process that broadly describes the production of parts by building up the material. There are multiple processes that can be used in AM, but this analysis will use the Direct Metal Laser Sintering (DMLS) process. The DMLS process falls under the category of the Powder Bed Fusion (PBF) processes in which parts are created by melting layers of powder particles together. DMLS builds the part by sintering, or melting together, layers of metal powder using a laser. In order to build the part, a 3D CAD model(stereolithography file, .stl) must be loaded into the manufacturing machine. The machine, an EOS GmbH M 280 DMLS for this study, takes the 3D model and slices it into layers. The part is then constructed by building each of these layers one on top of the other. The manufacturing process begins by coating the build plate with a thin layer of powder, and the first layer of the part is created when the laser sinters the powder together in the shape of the first layer. The unsintered powder remains in place to act as support material for the next layer. A new coating of powder is then rolled out across the build plate, and the second layer is sintered on top of the first layer. The sintering process forms the second layer and essentially welds the new layer to the previous layer. The process continues layer by layer until the part is completed. The part is then removed from the build chamber and all of the remaining powder is recycled. The ability to reuse the unsintered powder of the DMLS process results in significantly less waste than the traditional manufacturing and machining of wrought material.

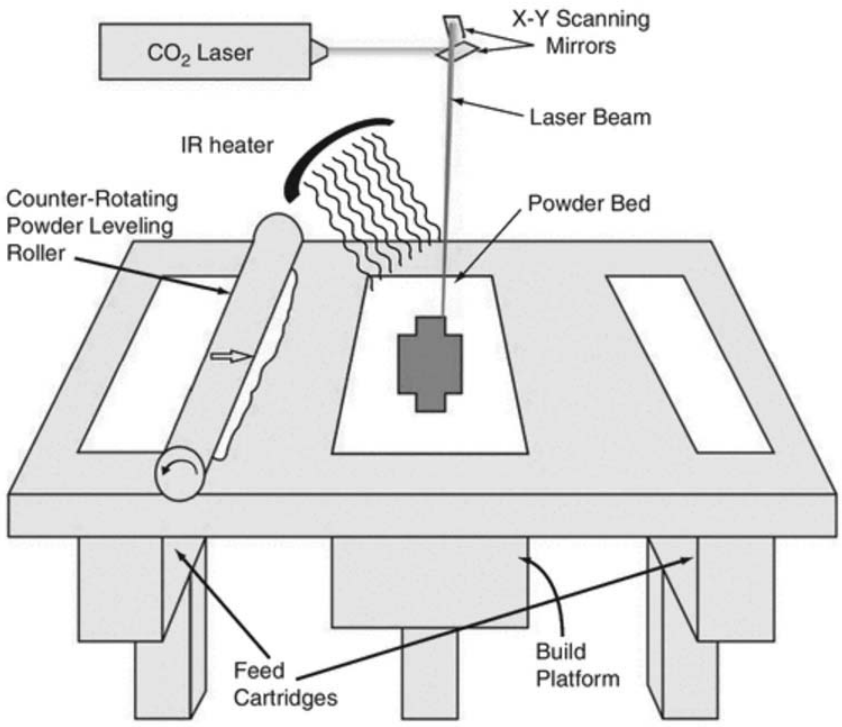

Figure 2.3. Powder Bed Fusion Process[1]

This process contains numerous variables such as the laser spot size, energy pulse duration, speed of the scan, spacing between melt pools and pattern of the scan. The other main variable is the powder being used. The shape, size and distribution of the power can have significant effects on the manufacturing process and introduce a large amount of variability. The large number of variables and the lack of standardization of the AM industry often results in parts made from the same material that have different properties[1]. Using this technique, parts are built using 2 different orientations, vertical or horizontal. Using a cylinder as an example, a vertical build consists of multiple circular, or penny shaped, layers built one upon the other until the part is finished as shown in 2.4a. A horizontal build consists of rectangular shaped layers that are built one upon the other until the part is finished as shown in 2.4b. This new process is much different from the standardized process that has been developed for wrought material[10].

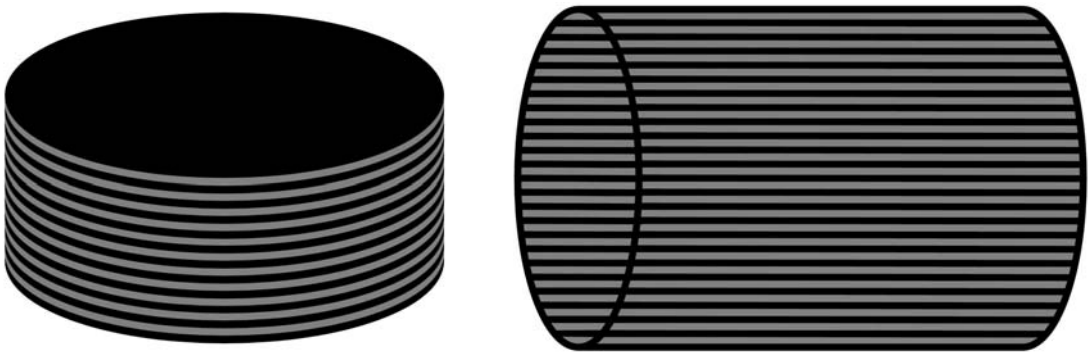

(a) Vertical Build Orientation **(b) Horizontal Build Orientation**

Figure 2.4. DMLS Build Orientation

The most significant difference between the process of DMLS and the traditional wrought process is the rapid heating and cooling cycles that the material undergoes throughout the DMLS. The strength of steels is highly dependent upon the microstructure, and the microstructure is dependent upon the heat treatment the material undergoes. It has been proven that the rapid heating and cooling cycles of steel produce a very fine grain structure and as the grain size decreases the strength and hardness increase[4]. This process suggests that the DMLS process will produce a fine grain structure for the material that should provide high strength and hardness.

2.3 Quasi-Static Compression and Tensile Testing

Quasi-static testing is one of the most popular material characterization techniques. It is used across a large variety of materials to determine their Yield Strength (YS), Ultimate Tensile Strength (UTS), Young's Modulus (E), toughness, and Failure Strain (FS). The testing is conducted by applying either a tension, or compression load onto the test specimen. The load is applied very slowly, keeping the strain rate very small (10^{-4} to 10^{-2} s^{-1})[11]. A strain gauge or extensometer is used to measure the deformation of the specimen as the load increases until the specimen fails, or the preset limit for the test is hit. The data measured from the test is used to create the

stress vs strain curve.

2.4 Digital Image Correlation

Digital Image Correlation (DIC) is an optical technique used for analyzing the deformation of objects. In the early 1980's it was proven that numerical algorithms could be written to measure the changes in images that can be used to calculate the deformations of a surface. Over the next decade the the procedures were validated, modified and improved while the numerical algorithms were improved and refined. DIC is a non-contact technique that can be used to calculate the displacement and strain of an object by measuring the change that occurs between images. A stochastic pattern is typically used to create markers on a surface that can then be tracked between images as shown in figure 2.5.

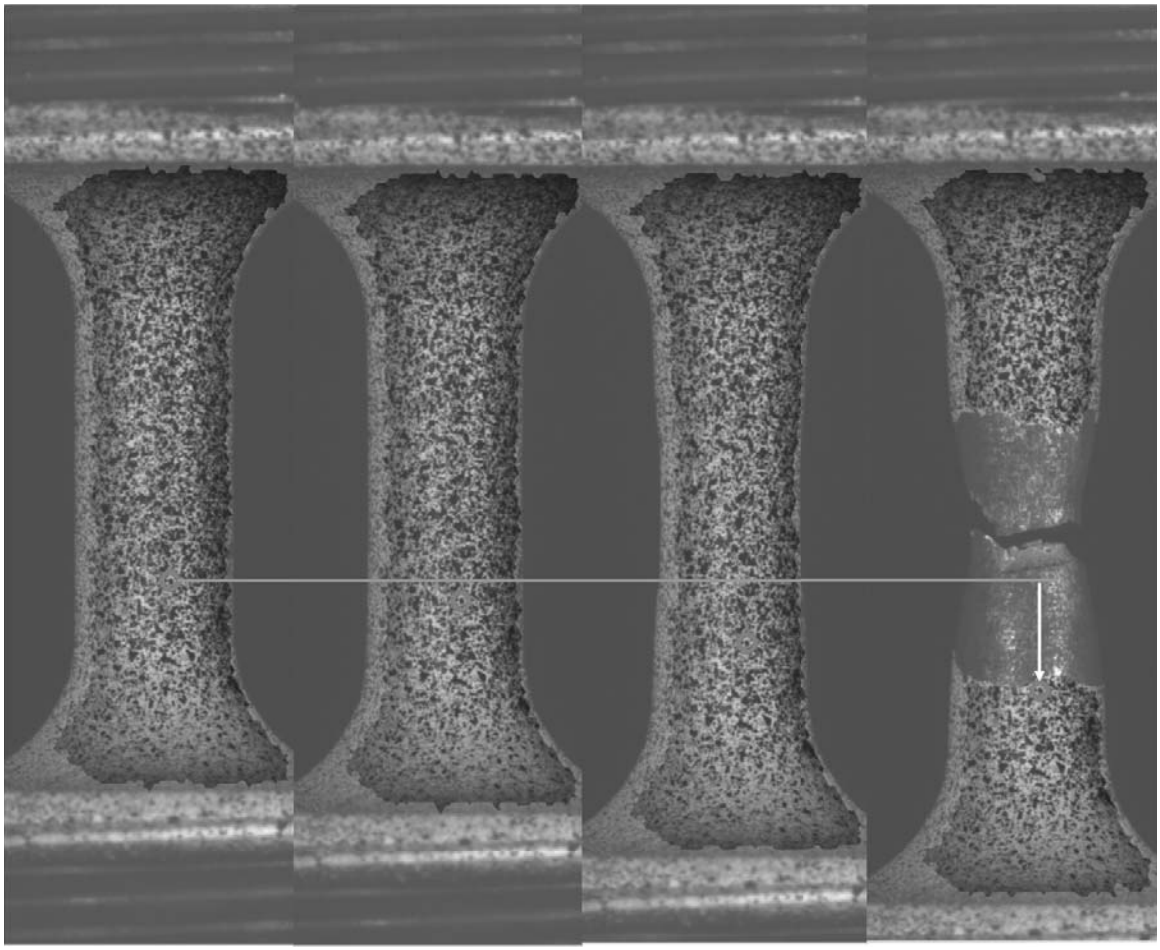

Figure 2.5. Simple DIC method for tracking marker movement to show linear displacement

A numerical algorithm analyzes the part and identifies the specific points of interest that can be tracked. As the software moves from image to image, it is able to calculate how far each unique point moves and can convert that deflection into displacement and strain.[12] For this testing the GOM Correlate software is used to calculate the displacement and strain of the specimen during testing. Prior to testing, a calibration is conducted that enables the software to measure the exact distance of each pixel. The software is then able to calculate point and full field displacements and strain across the surface.

2.5 Split Hopkinson Pressure Bar

The SHPB was originally developed as a technique to measure the pressure waves of explosives or high speed bullet impacts. As they developed the technique, they found they could measure the impact stress wave propagation through materials. In 1949 Herbert Kolsky further refined the technique and discovered that he could measure the dynamic stress-strain response of materials. With the development of new technology and further understanding of the propagation of the compressive wave through a bar, the SHPB test method has evolved into the standard test apparatus for measuring the mechanical response of material deforming at high strain rates. A general SHPB apparatus is shown in figure 2.6.

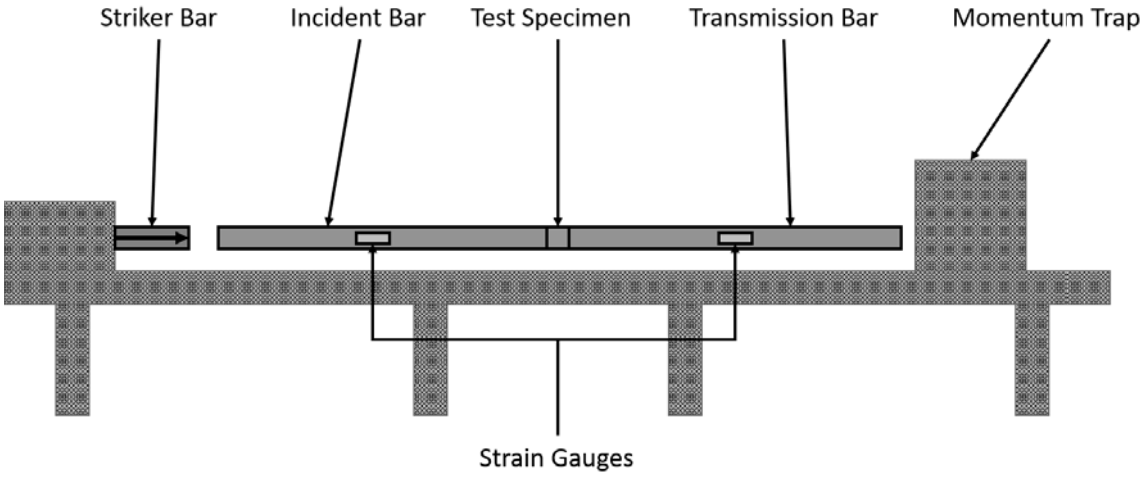

Figure 2.6. General SHPB apparatus

The SHPB is generally composed of 5 main parts: the striker, incident bar, transmission bar, momentum trap and data acquisition system. The striker is used to create the dynamic load, and is typically a pneumatic gun that fires a striker bar into the incident bar in a repeatable manner. The size and velocity of the striker can by changed to achieve the desired strain rate. The striker, incident and transmission bars are made of long elastic bars of the same material and same diameter. The three

bars are mounted and aligned so that they are free to move in the axial direction. The impact of the striker on the incident bar creates a compressive stress wave that travels through the incident bar towards the test specimen. The impact also creates a compressive stress wave in the striker bar. When the compressive wave in the striker bar reaches free end the wave is reflects back into striker bar as a tension wave that unloads the striker bar. The duration of the loading can then be calculated as the time it takes the compressive wave to travel twice the length of the striker bar, as shown in 2.1 where T is the duration, L_st is the length of the striker and C_st is the elastic wave speed in the striker bar.

$$T = \frac{2L_{st}}{C_{st}} \tag{2.1}$$

Upon reaching the interface between the incident bar and the test specimen, a portion of the wave is reflected back into the incident bar and the rest of the wave continues into the test specimen. The compressive wave inside the specimen is reflected back and forth inside the specimen due to the wave impedance mismatch between the test specimen and the incident and transmission bars. With each reflection of the stress wave inside the test specimen the stress increases, and the increasing stress results in deformation of the test specimen. The interaction between test specimen and the transmission bar transmits the strain history of the test specimen. The path of the compressive wave is shown in figure 2.7. The momentum trap is used to absorb the momentum of the system, de-loading the incident bar, test specimen, and transmission bar[13]. If desired the SHPB set up can also be modified to conduct indirect tension tests.

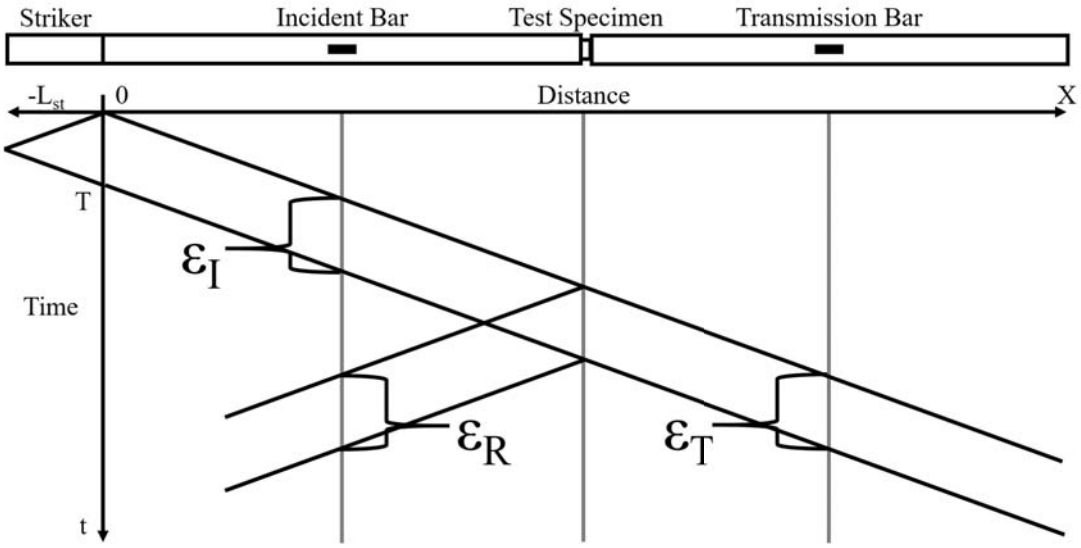

Figure 2.7. Wave propagation during SHPB test

The data acquisition system measures the strain caused by the compression wave in the incident bar and the transmission bar. These strain values can then be used to calculate the strain rate, strain, and stress of the test specimen. The average stress that the specimen feels can be expressed in terms of the forces being exerted on each end of the specimen. Figure 2.8 shows the forces, strains and velocity at the interfaces.

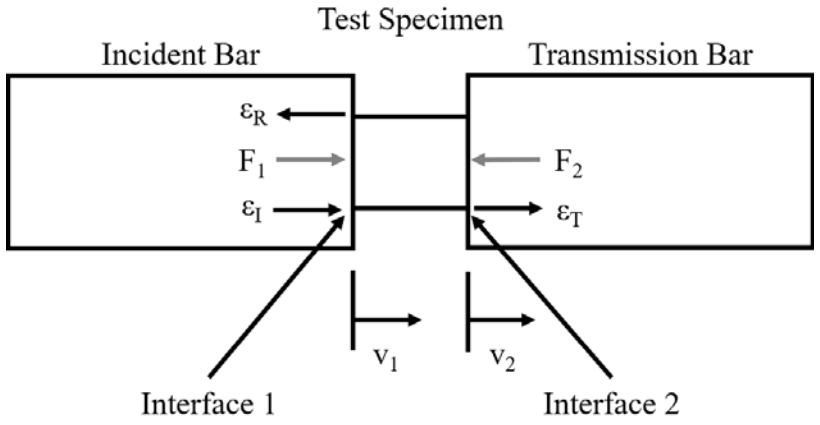

Figure 2.8. Specimen interface with incident and transmission bars

The average force on the specimen is then given by:

$$F_{\mathrm{AVG}}(t) = \frac{F_1(t) - F_2(t)}{2} \tag{2.2}$$

The average stress on a cylindrical specimen is:

$$\sigma_{\mathrm{AVG}}(t) = \frac{F_{\mathrm{AVG}}(t)}{\frac{\pi D_S^2}{4}} \tag{2.3}$$

Where D_S is the instantaneous diameter of the specimen. The forces F_1 and F_2 acting on the specimen are due to the incident and transmission bars. For a specimen in dynamic equilibrium, the forces on the ends of the pressure bars can be expressed in terms of the incident and transmitted pressure bar.

$$F_1(t) = E_{BAR}[\epsilon_I(t) + \epsilon_R(t)]\frac{\pi D_{BAR}^2}{4} \tag{2.4}$$

$$F_1(t) = E_{BAR}\epsilon_T(t)\frac{\pi D_{BAR}^2}{4} \tag{2.5}$$

Where ϵ_I is the strain of the incident bar, ϵ_R is the strain reflected back into the incident bar, and ϵ_T is the strain of the transmitted bar. By combining equations 2.2, 2.3, 2.4 and 2.5, the average stress on the specimen can be given in terms of the pressure bar strains.

$$\sigma_{\mathrm{AVG}}(t) = \frac{E_{BAR}D_{BAR}^2}{2D_S^2}[\epsilon_I(t) + \epsilon_R(t) + \epsilon_T(t)] \tag{2.6}$$

If the specimen deforms uniformly the strains in the incident bar are equal to the strains in the transmitter bar.

$$\epsilon_I(t) + \epsilon_R(t) = \epsilon_T(t) \tag{2.7}$$

Then the average specimen stress can be reduced to:

$$\sigma_{\mathrm{AVG}}(t) = \frac{E_{BAR} D_{BAR}^2}{D_S^2} \epsilon_T(t) \tag{2.8}$$

In order to calculate the strain of the test specimen, we must understand how the pressure wave travels through the transmitter bar and into the specimen. For simplicity in the calculations, the incident bar and transmitter bar have the same cross section (which is constant) A_{BAR}, modulus of elasticity E_{BAR}, and density ρ_{BAR}. For elastic bars these stresses are related to the strains by Hookes law. Furthermore, these strains can be expressed in terms of the displacements, u. For a thin long bar the equation of motion for the axial displacement, u, is given by:

$$C_{BAR}^2 \frac{\partial^2 u_1}{\partial x^2} = \frac{\partial^2 u_1}{\partial t^2} \tag{2.9}$$

Where C_{BAR} is the Elastic Wave Speed of the incident and transmission Bars. Recognizing that $\frac{\partial^2 u}{\partial t^2}$ is equal to $\frac{\partial v}{\partial t}$ where v is the particle velocity we can then express the particle velocity in terms of the bar strain as

$$v = C_{BAR} \epsilon \tag{2.10}$$

And for a negative traveling wave the velocity is

$$v = -C_{BAR} \epsilon \tag{2.11}$$

Knowing the particle velocity in terms of the pressure bar strains we can now calculate the specimen strain rate. The average strain rate at any time is

$$\frac{\partial \epsilon}{\partial t} = \frac{v_1 - v_2}{L_S} \tag{2.12}$$

The velocity of interface 1 is the velocity of the incident wave, and the reflected wave

$$v_1 = C_{BAR}\epsilon_I - C_{BAR}\epsilon_R = C_{BAR}(\epsilon_I - \epsilon_R) \tag{2.13}$$

The velocity of interface 2 is then calculated with the strain of the transmitter bar

$$v_2 = C_{BAR}\epsilon_T \tag{2.14}$$

Knowing the strains in the incident bar are equal to the strains in the transmitter bar, we can find an expression for the specimen strain rate in terms of the pressure bar strains

$$\frac{\partial \epsilon}{\partial t} = \frac{C_{BAR}(\epsilon_T - \epsilon_I + \epsilon_R)}{L_S} = -\frac{2C_{BAR}\epsilon_R}{L_S} \tag{2.15}$$

The specimen strain can then be calculated by integrating over time to get

$$\epsilon_S(t) = -\frac{2C_{BAR}}{L_S}\int_0^t \epsilon_R(t)\,\mathrm{d}t \tag{2.16}$$

The theory presented above is based on the assumption that the specimens only undergo one dimensional wave propagation. They are derived from the conservation of mass and momentum with engineering measurements.

2.6 Optical Microscopy

Optical microscopy will be used to make a general analysis of the effects of AM on the microstructure that is visible to the eye. Optical microscopy relies on the proper surface preparations in order to reveal the important details. The main method for optical microscopy is to polish the specimen as smooth as possible to remove scratches or anomalies. The polished surface is then etched, a technique in which the top layer of the specimen is chemically removed. The etching process removes atoms around

the grain boundaries more easily than from the center of the grain. This makes the grain boundaries more visible. This will show the visible effect that the AM process has on the manufacturing process of the stainless steel.

2.7 Energy Dispersive X-ray Spectroscopy

EDS is a material characterization technique that is used to determine the elemental composition of a material. The techniques fires a beam of electrons from a Scanning Electron Microscope (SEM) into the specimen which the emits x-rays. After the sample is loaded into the SEM it is positioned so that the beam of electrons is fired incident to it. When the beam of electrons impact the specimen the incoming electrons may collide with an electron of the specimen. If the incoming electron has enough kinetic energy, it will knock the electron free of its shell. When an inner shell electron is knocked free an electron from a higher energy shell will transition down to replace it. When the high energy electron transitions to the lower energy shell, it most lose some of its own energy, which it does as a photon in an x-ray. The energy of these x-rays are characteristic of the element that is emitting it. By measuring the energy of the x-ray, the element it is released from can be determined. The typical EDS system is incorporated into an SEM and requires an x-ray detector, pulse processing circuitry and analyzer equipment[14]. When detector is struck by an x-ray it creates a charge pulse that is converted into a voltages pulse that can be analyzed for the energy level of the x-ray. The analyzer equipment counts every detect that it receives and is able to associate each x-ray with a specific element. The energy level of the x-rays even if they are given off by electrons transitioning from different shell levels. By counting all of the x-rays emitted, the concentration of each element can be calculated. EDS is excellent at detecting all of the elements that make up the composition of the specimen, but the typical accuracy of EDS is approximately 2%.

When the composition of the specimen is known, the accuracy can be increased by calibrating for the know composition. EDS does struggle to detect the low energy x-rays of carbon, nitrogen and oxygen[15].

2.8 Electron Backscatter Diffraction

EBSD is a materials characterization technique that is used to analyze material microstructure. EBSD uses the electron beam from a SEM to collect the crystallographic information about a test specimen[16]. The specimen is loaded into the SEM and positioned appropriately so that the electrons diffracting from the sample strike a detector plate. When the SEM fires a beam of electrons at a crystal, the electrons will penetrate the crystal to a depth that depends on the power of the beam. Some of the electrons that penetrate the material will bounce off the internal structure of the crystal and escape. These electrons escape at certain angles, Bragg angles, related to the lattice structure of the material. The escaping electrons are then detected by the SEM and form Kikuchi patterns as shown in figure 2.9a. The SEM is then able to analyze the Kikuchi patterns and determine the type of lattice structure. By scanning the specimen with this technique, the SEM is able to determine what type of crystal the specimen is made of. It can also detect the size, and orientation of the grains in the microstructure as shown in figure 2.9b. The figure shows the grain boundary, orientation and the grain size. The combination of grain size and orientation plays a major role in indicating the internal resistance of a material to external forces. It has been shown that the internal deformation can be a gauge for determining viscoplastic restraint. A source of interest is how the formation of the internal structures affects the material response to compressive loading. There is concern that the DMLS method affects the internal resistance of the material as a byproduct of the material microstructure formation through the build.

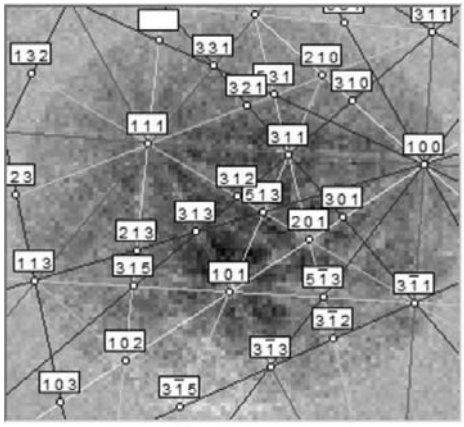

(a) Kikuchi Pattern that is used to determine the crystal structure

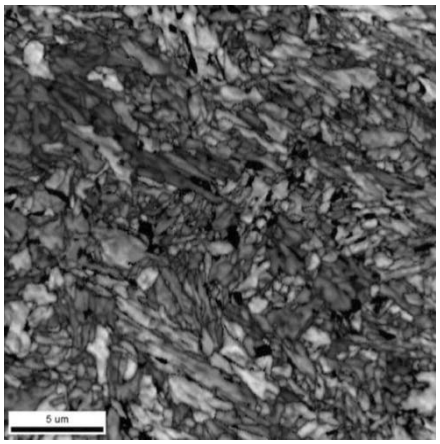

(b) EBSD micrograph showing the size and orientation of individual crystals within the material

Figure 2.9. Electron Backscatter Diffraction

III. Research Methodology

Chapter three establishes the materials and the methods used for the study and is broken into 4 sections. This first section will discuss the material that is used to create the specimens and the method of manufacture. The second section will discuss the specific heat treatments that the samples will undergo. The third section will review each method of testing as well as the set up of each test apparatus. The size and shape of the test specimens for each test will also be established. The last section will review how the microstructural analysis samples will be prepared for EBSD and EDS.

3.1 Material

The objective of this research is to establish the mechanical properties of AM 15-5PH stainless steel. In order to be able to characterize any effect the new manufacturing method may have on the material, the material must be representative of material that could potentially be purchased, so a third party manufacturer was selected to build samples, I3DMFG. This verified that the parts would be created using the same parameters that would be suggested by a manufacturer. This is the same manufacturer, and build parameters as was used by Dempsey[17], which enables a comparison between the data collected in her effort and this effort.

The parts were manufactured using the Electro Optical Systems (EOS) EOSINT M 280 system. The M280 system was released in 2010 and is a widely used system in the AM industry. The M 280 can produce parts from a variety of material such as aluminum, cobalt chrome, maraging steel, stainless steels, and titanium using either a nitrogen or argon environment. This study used a single build to produce all of the samples required for testing. The build used the EOS Stainless Steel PH1 powder

that conforms to the AISI standards of 15-5 PH (UNS15500) that is provided by a third party vendor. When manufacturing a part, the power of the laser determines how much energy is transferred into the powder and must be high enough to fully melt the powder and sinter it to the surrounding material creating a fully dense part. It is essential to keep the power as low as possible because excessive energy results in over-sintering, which creates defects in the part, and can build up excess heat in the part that could result in residual heat stress. The hatching distance is determined as the distance between laser passes. The ideal setting for the hatching distance allows for one quarter of the laser diameter to overlap the previous pass insuring full sintering between new passes and previous passes. The scan speed determines how fast the laser passes over the part. The scan speed combines with the power to determine how much energy is transferred into the material. The layer thickness is one of the most important parameters. It determines how thick each layer will be which determines how much energy is need to sinter the layer[18]. Thinner layers ensure the powder will fully melt to create a fully dense part, but also increase the build time. The parameters used for building theses test specimens are shown in table 3.1.

Parameter	Value
Laser Power	195 W
Scan Speed	1000 mm/s
Hatching Distance	0.15 mm
Overlap	0.12 mm
Beam Offset	0.015 mm
Layer Thickness	.04 mm

Table 3.1. Build Parameters

The samples made for this thesis will be from a single build to make sure the properties are they same across all the test samples. In order to understand how the build orientation may effect the strength of the material The samples will be constructed in two different build orientations. Half of the samples will be built in

the vertical orientation. The vertical orientation creates the part by constructing it from penny shaped layers that are sintered together as shown in figure 2.4a. Half of the samples will be built in the horizontal orientation. The horizontal orientation constructs the part from rectangular shaped layers that are sintered together as shown in figure 2.4b.

3.2 Heat Treatment

Martensitic PH stainless steels are typically delivered to customers in Condition A. Condition A is when the material is in its softest form so that it is most easily machinable. Condition A is reached by solution annealing the steel at 1900 °F and water quenching. The solution anneal homogenizes the steel providing uniform properties as well as allowing the copper to diffuse within the iron. Upon water quenching the material cools through a diffusion-less process that results in the martensitic structure. Condition A is comparable to what manufacturers refer to as the as-built condition. The as built condition is the condition the material is in after being manufactured. The subsequent heat treatments that 15-5 PH material goes through are H900, H1025, or H1150 as defined by the AISI[9]. The H900 heat treatment used in this study heated the samples to 900 °F and held the samples at this temperature for 4 hours, then the specimens were air cooled. Specimens undergoing the H1025 heat treatment were heated to 1025 °F and held the samples at this temperature for 4 hours, then the specimens were air cooled.

3.3 Mechanical Properties Testing

3.3.1 Quasi-Static Testing

Quasi-static compression testing was conducted using an Instron 1332 was used to conduct the compression tests. Compression testing was conducted using a controlled

constant strain rate of 10^{-3} s^{-1} until a maximum strain of 30% was reached. Stress and displacement were recorded and used to calculate the stress vs strain curve, yield stress and modulus of elasticity. Quasi static compression testing was conducted at 4 specific conditions as shown in figure 3.2

Compression Testing		
Test Condition	Heat Treatment	Orientation
1	Condition A	Vertical
2	Condition A	Horizontal
3	H900	Vertical
4	H900	Horizontal

Table 3.2. Quasi Static Compression Test Points

The test specimens for the quasi-static compression testing will be machined from a larger rod that is printed. This ensures that the surface roughness is uniform across all of the test specimens, and that the surface roughness does not affect the test results. The machining process also removes any micro cracks that may form at the edges of the printed materials. The material will be printed as rods shown in figure 3.1a and machined into test specimens as shown in figure 3.1b for the vertical specimens, and as shown in figure 3.1a and 3.1b for the horizontal specimens.

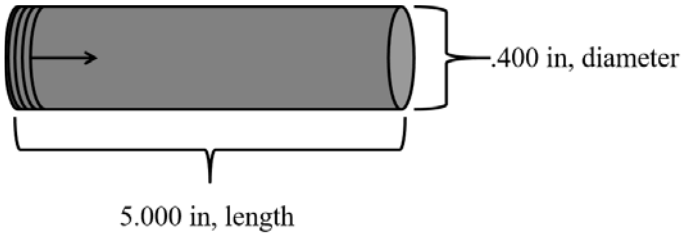

(a) Vertical orientation raw material rod for quasi-static compression testing dimensions

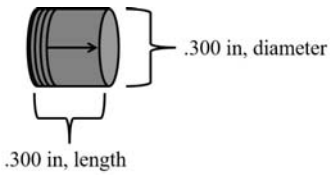

(b) Vertical orientation quasi-static compression testing specimen dimensions

Figure 3.1. Vertical quasi-static compression testing specimens

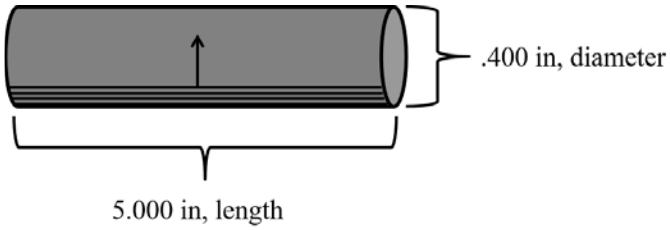

(a) Horizontal orientation raw material rod for quasi-static compression testing dimensions

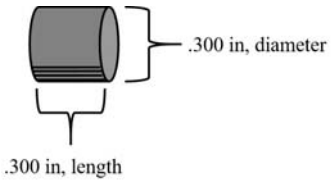

(b) Horizontal orientation quasi-static compression testing specimen dimensions

Figure 3.2. Horizontal quasi-static compression testing specimens

Quasi-static tension testing was also conducted using the Instron 1332. A constant strain rate of 10^{-3} s^{-1} was used until the specimen surpassed the yield strength point. The strain rate was then increased to 4 x 10^{-3} s^{-1} until the specimen fractured. Stress and displacement were recorded and used to calculate the stress vs strain curve, yield stress, ultimate stress and modulus of elasticity. Quasi static tension testing was conducted at 4 specific conditions as shown in figure 3.3

Tension Testing		
Test Condition	Heat Treatment	Orientation
5	Condition A	Vertical
6	Condition A	Horizontal
7	H900	Vertical
8	H900	Horizontal

Table 3.3. Quasi Static Tension Test Points

The test specimens for the quasi-static compression testing will be machined from a larger rod that is printed. This ensures that the surface roughness is uniform across all of the test specimens, and that the surface roughness does not affect the test results. The machining process also removes any micro cracks that may form at the edges of the printed materials. The material will be printed as rods shown in figure 3.3a and machined into test specimens as shown in figure 3.3c for the vertical specimens, and as shown in figure 3.3b and 3.3c for the horizontal specimens.

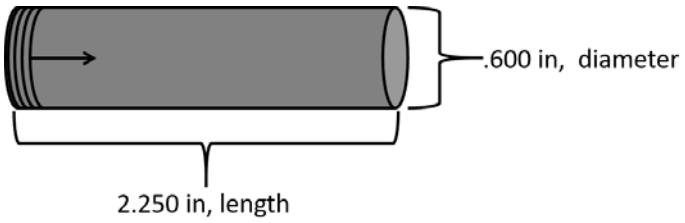

(a) Vertical orientation raw material rod for quasi-static tension testing dimensions

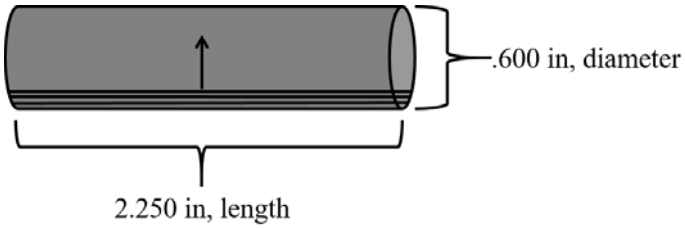

(b) Horizontal orientation raw material rod for quasi-static tension testing dimensions

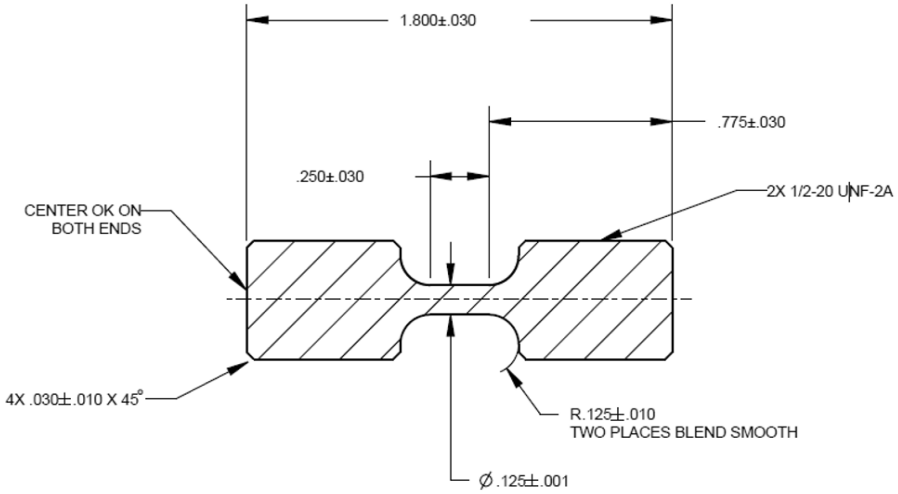

(c) Horizontal and vertical orientation quasi-static tension testing specimen dimensions

Figure 3.3. Quasi-static tension testing specimen dimensions

During the quasi-static tension and compression testing DIC data will also be collected to. The DIC data will be used to confirm the Instron results. The images will be analyzed using the GOM Correlate software to determine the deformation and strain of test specimens during testing.

3.3.2 Split Hopkinson Pressure Bar Testing

The SHPB test apparatus is a very specialized device, and as a result there is no established standards for testing. This testing effort covers SHPB testing in compression which uses a similar set up as outlined in the SHPB theory. Results from Dempsey's[17] SHPB direct tension testing will also be included. The specifications for the compression testing apparatus are shown in table 3.4 and the specifications for the tension testing apparatus are shown in table 3.5.

SHPB Compression Test		
	Incident	Transmission
Material	C300 Maraging Steel	C300 Maraging Steel
Length (in)	120.00	120.00
Diameter (in)	0.750	0.750
Young's Modulus (psi)	28282358	28282358
Wave Speed (in/sec)	189448	189448

Table 3.4. SHPB Compression Testing apparatus specifications

SHPB Direct Tension		
	Incident	Transmission
Material	AL 7075-T6	AL 7075-T6
Length (in)	144.00	144.00
Diameter (in)	1.00	1.00
Young's Modulus (psi)	10442000	10442000
Wave Speed (in/sec)	207480	207480

Table 3.5. SHPB Compression Testing apparatus specifications

The test specimens for the SHPB compression testing will be machined from a larger rod that is printed. This ensures that the surface roughness is uniform across

all of the test specimens, and that the surface roughness does not affect the test results. The machining process also removes any micro cracks that may form at the edges of the printed materials. The material will be printed as rods shown in figure 3.4a for vertical specimens and 3.4b for horizontal specimens. Test specimens of the dimension showed in figure 3.4c will be machined from each rod.

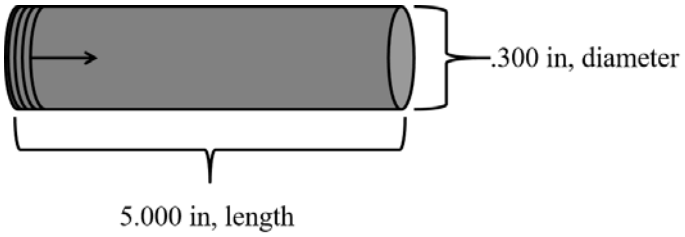

(a) Vertical orientation raw material rod for SHPB compression testing dimensions

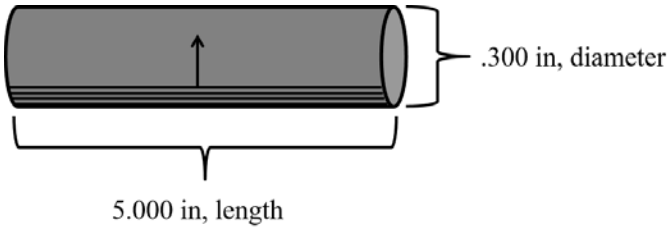

(b) Horizontal orientation raw material rod for SHPB compression testing dimensions

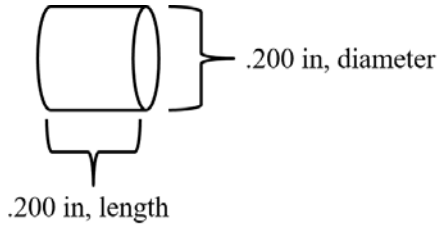

(c) Horizontal and vertical orientation SHPB compression testing specimen dimensions

Figure 3.4. SHPB compression testing specimen dimensions

The tension SHPB testing conducted by Dempsey[17] was conducted using the same methodology. The test specimens are machined from larger rods that were built by AM. This ensures that the surface roughness is uniform across all of the test specimens, and that the surface roughness does not affect the test results. The

machining process also removes any micro cracks that may form at the edges of the printed materials. The material will be printed as rods shown in figure 3.4a for vertical specimens and 3.4b for horizontal specimens. Test specimens of the dimension showed in figure 3.4c will be machined from each rod.

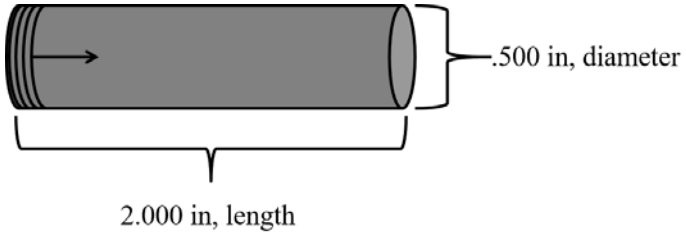

(a) Vertical orientation raw material rod for SHPB tension testing dimensions

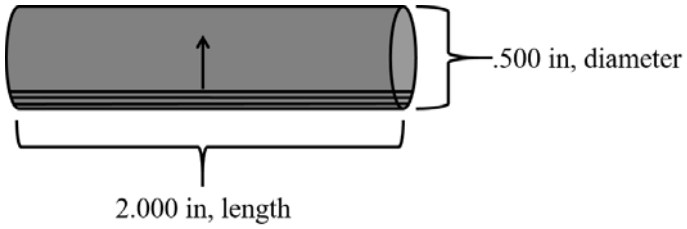

(b) Horizontal orientation raw material rod for SHPB tension testing dimensions

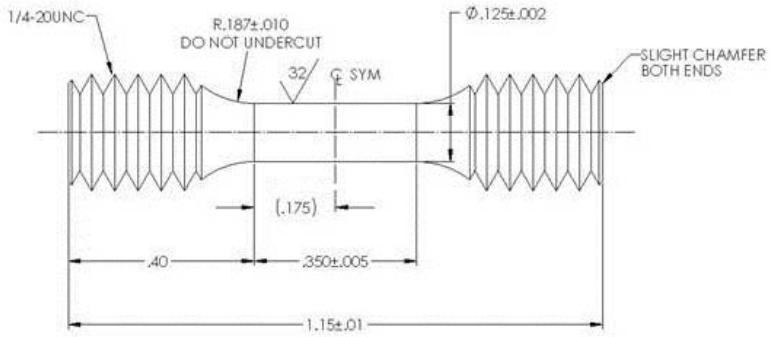

(c) Horizontal and vertical orientation SHPB tension testing specimen dimensions

Figure 3.5. SHPB tension testing specimen dimensions

In order to fully investigate the material, test points were chosen across heat treatment, build orientation and at two strain rates With the quasi-static testing

investigating the low strain rate the SHPB analyzed a low and high strain rate. The low strain rate was selected as 500 s^{-1} and the high strain rate was selected as 800 s^{-1}. These strain rates were the same as those investigated by Dempsey[17] in order to make a comparison of the data. The test points for the compression testing is shown in table 3.6 and the tension testing that was completed by Dempsey is shown in table 3.7.

Compression Testing			
Test Condition	Heat Treatment	Strain Rate	Orientation
9	Condition A	500 s^{-1}	Vertical
10	Condition A	500 s^{-1}	Horizontal
11	Condition A	800 s^{-1}	Vertical
12	Condition A	800 s^{-1}	Horizontal
13	H900	500 s^{-1}	Vertical
14	H900	500 s^{-1}	Horizontal
15	H900	800 s^{-1}	Vertical
16	H900	800 s^{-1}	Horizontal

Table 3.6. SHPB compression test points

Tension Testing			
Test Condition	Heat Treatment	Strain Rate	Orientation
17	As Built	500 s^{-1}	Vertical
18	As Built	500 s^{-1}	Horizontal
19	As Built	800 s^{-1}	Vertical
20	As Built	800 s^{-1}	Horizontal
21	H900	500 s^{-1}	Vertical
22	H900	500 s^{-1}	Horizontal
23	H900	800 s^{-1}	Vertical
24	H900	800 s^{-1}	Horizontal
25	H1025	500 s^{-1}	Vertical
26	H1025	500 s^{-1}	Horizontal
27	H1025	800 s^{-1}	Vertical
28	H1025	800 s^{-1}	Horizontal

Table 3.7. SHPB tension test points

3.4 Microstructural and Energy Dispersive X-Ray Spectroscopy Testing

3.4.1 Sample Preparation

The microstructure of the material plays an important role in controlling the strength of the material. In order to accurately characterize the microstructure, the samples must be properly polished in order for the grain structure to be visible. Test specimens were mounted into a conductive phenolic compound and pressed to 1.25 in. diameter cylinder. The samples were then ground and polished. Fine grinding was accomplished using a poly crystalline diamond suspension followed by a finer diamond suspension. After grinding the samples were polished with a colloidal silica.

Samples will be analyzed as either in plane, the image is taken of the build plane, or out of plane, the image is taken across multiple build planes. Figure 3.6 shows an example of both in plane and out of plane for the vertical specimens, and figure 3.7 shows an example of both in plane and out of plane for horizontal specimens. Microscopy will be completed on both untested and tested samples to evaluate the microstructure.

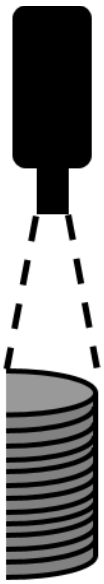

(a) Microscopy image of a vertical orientation specimen in the build plane

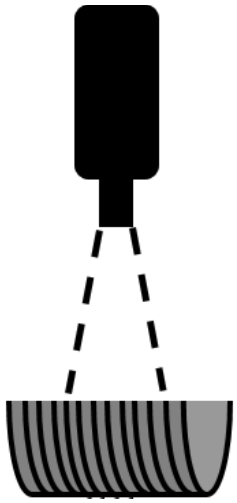

(b) Microscopy image of a vertical orientation specimen perpendicular to the build plane

Figure 3.6. Microscopy orientation of vertical specimens

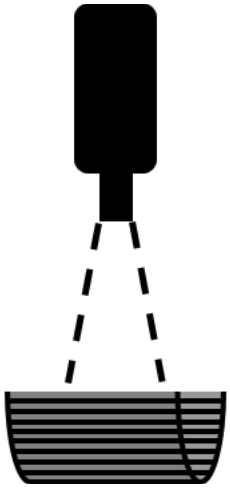

(a) Microscopy image of a horizontal orientation specimen in the build plane

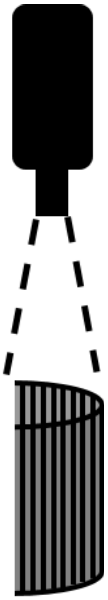

(b) Microscopy image of a horizontal orientation specimen perpendicular to the build plane

Figure 3.7. Microscopy orientation of horizontal specimens

3.4.2 Energy Dispersive X-Ray Spectroscopy

EDS is used to confirm the composition of the testing material to verify that it falls within the AISI standards. EDS testing will be complete on an untested sample from the build. Because carbon, nitrogen and oxygen generate low energy x-rays that are difficult to detect at low concentrations, the EDS testing will be used only to calculate the percent weight of Mn, Si, Cr, Ni, Mo, Nb, Cu, and Fe. Testing will be conducted using a Quanta 200 FEG.

3.4.3 Electron Backscatter Diffraction

EBSD will be used to take micrographs of the specimens to analyze the microstructure. EBSD is a tool for determining the atomic arrangement of the material and is able to identify the individual grains of the material as well as their orientation. This allows an analysis on the grain size of the samples. Testing will be conducted using a Quanta 200 FEG.

IV. Results

The objective of this research is to establish the mechanical properties of AM 15-5PH stainless steel. The directed research analyzed and compared the mechanical material properties of AM 15-5PH stainless steel in compression and tension. The three variables that were changed to fully characterize the material were the build orientation, heat treatment and strain rate. Test specimens were purchased through a third party manufacturer in accordance to their recommended build specifications, making the samples representative of the industry. The quasi-static, and compression SHPB test specimens were all built in a single build, and the samples for the tension SHPB were from a different build. To fully characterize the effect of AM on the material properties, the microstructure will be analyzed to see how the microstructure responds to the DMLS process.

Chapter four is broken into five sections. Section one will discuss the quasi-static testing and the DIC data that was collected during the quasi-static testing. Section two will review the results of the SHPB compression testing and the SHPB tension testing completed by Dempsey[17]. Section three will review the results of the microstructural analysis. This will include the results from the optical microscope, EDS, and EBSD. Section 4 will analyze the results of the mechanical testing. And section five will analyze the results of the microstructural testing.

4.1 Quasi-Static Compression and Tension Testing

Quasi-static testing was conducted at each of the 4 metallurgical condition in both tension and compression. The Quasi-static testing was conducted to establish the typical strength of material values for the AM. The quasi-static data is also required in order to investigate the effect of strain rate on the material. Quasi-static testing

will be very useful for comparing the mechanical properties of the AM material to the properties of wrought material. It will also reveal any effects the build orientation and heat treatment have on the material. At each test point 4 specimens were tested to verify the repeatability of each test and identify any potential outliers.

4.1.1 Quasi-Static Compression Testing

The results of the quasi-static compression testing are stress vs strain curves. From these stress vs strain curves the modulus of Elasticity and the YS can be obtained. The stress vs strain curves for the quasi-static compression testing is shown in figure 4.1. Further analysis of the data calculated the modulus of elasticity and the 0.2 % YS. The YS results shown was calculated by forming a line with a slope equal to the Youngs modulus in the elastic region and offsetting it by 0.2% strain. The yield stress is then calculated the as the point where the offset line intercepts the stress-strain curve. The compression results are shown in table 4.1.

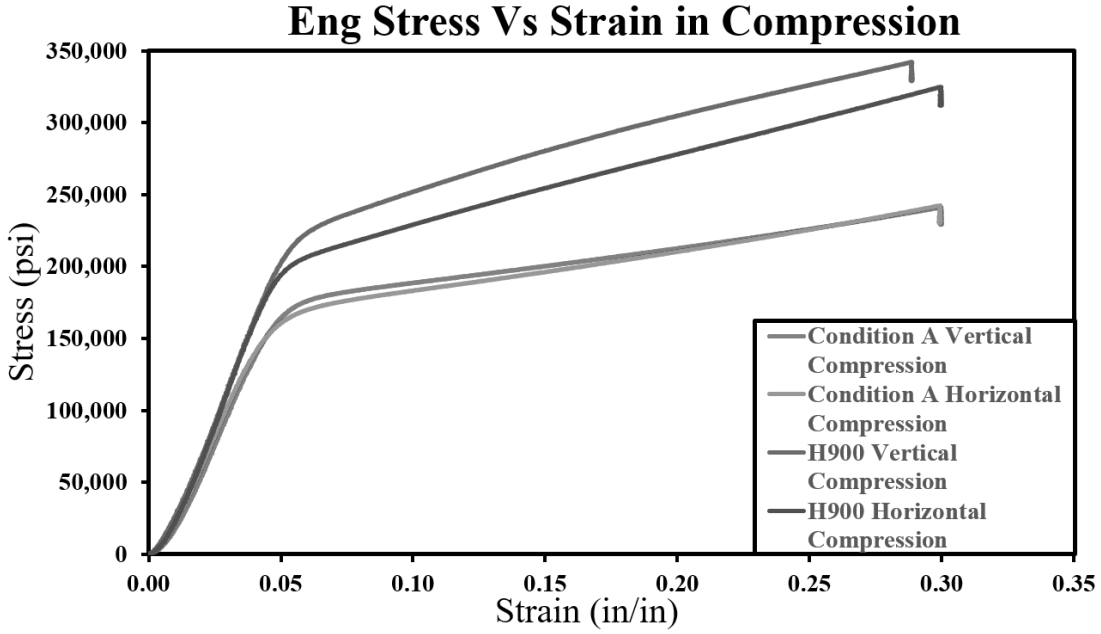

Figure 4.1. Quasi static compression engineering stress vs strain

Specimen	Yield Stress (psi)	E(Instron) (psi)	E(DIC) (psi)
Condition A H1	138446	4326165	N/A
Condition A H2	139456	4428011	N/A
Condition A H3	136594	4415632	N/A
Condition A H4	139078	4390533	N/A
Condition A H5	142731	4287799	18269822
Average	139261	4369628	18269822
Condition A V1	149452	4443006	N/A
Condition A V2	149453	4429066	N/A
Condition A V3	148002	4456666	N/A
Condition A V4	148897	4511644	N/A
Condition A V5	150588	4350703	24950866
Average	149278	4460096	24950866
H900 H1	182098	4945811	N/A
H900 H2	182208	5047581	N/A
H900 H3	184325	4951866	N/A
H900 H4	181005	4862566	N/A
H900 H5	183876	4938711	30991566
Average	182702	4951956	30991566
H900 V1	205429	5004811	N/A
H900 V2	201669	4971899	N/A
H900 V3	197653	5053317	N/A
H900 V4	203845	5098878	N/A
H900 V5	200929	4890944	30060744
Average	202149	5032226	30060744
AK Steel Condition A	140000	28500000	N/A
AK Steel H900	201000	28500000	N/A

Table 4.1. Quasi static compression results

The results revealed that the modulus of elasticity was significantly lower than expected, approximately one quarter of the expected value. This unexpected result led to further analysis of the strain. The original tests were accomplished without DIC, in order to investigate the strain an additional sample for each test point was tested using DIC. When the strain calculated from the Instron displacement was plotted with the strain measured from the DIC, there was a significant offset between the two, as shown in figure 4.2. The DIC data shows that strain does not increase at a linear rate during the initial application of the load and is significantly lower, as

shown in figure 4.3. As the load is applied to the specimen the Instron frame and load cell will deform in small amounts. The amount of deformation caused by the compliance in the Instron is typically very small, but can lead to significant errors in the test results when dealing with very stiff materials traveling small distances[19]. With the length of the test specimen at only 0.3 in, the relatively small amount of compliance deformation from the Instron results in a significant increase in the strain measured by the Instron. This increase in the strain resulted in the slope of the stress vs strain curve to be significantly reduced. Using the strain calculated from the DIC results in a significantly higher modulus of elasticity. In table 4.1 the E(Instron) refers to the modulus of elasticity calculated using the Instron strain, and E(DIC) refers to the modulus of elasticity calculated using the DIC strain. This effect can be seen in figure 4.4 in which the solid stress vs strain curves are calculated using the DIC strain and the dashed curves are the stress vs strain curves for the Instron.

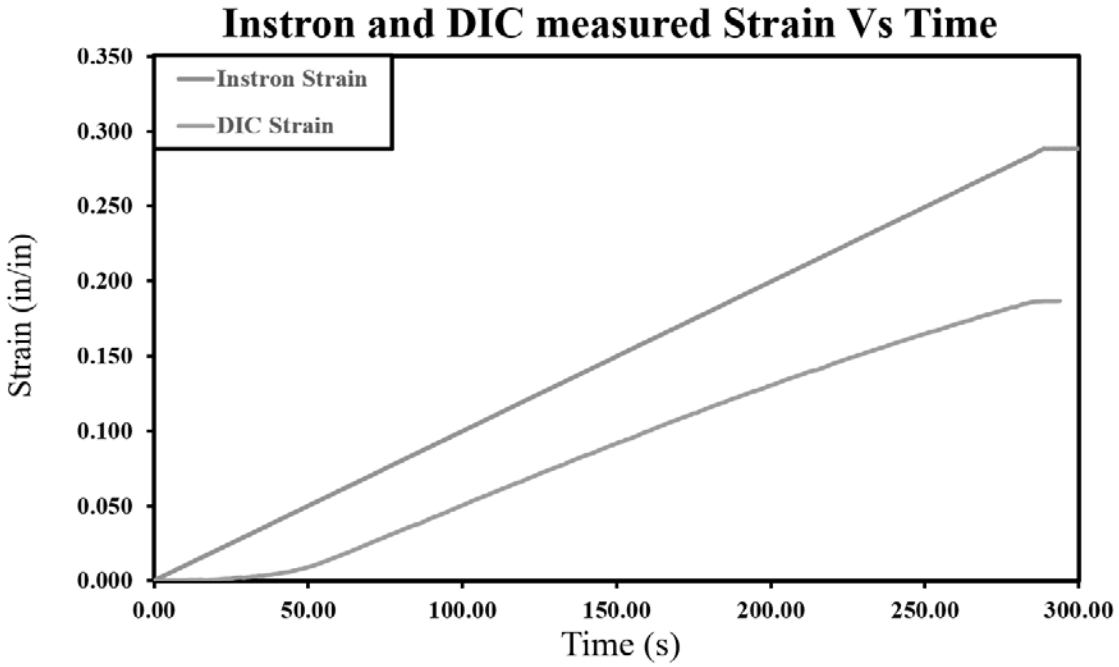

Figure 4.2. Significant error in the Compression Instron strain when conpared to the DIC strain vs time

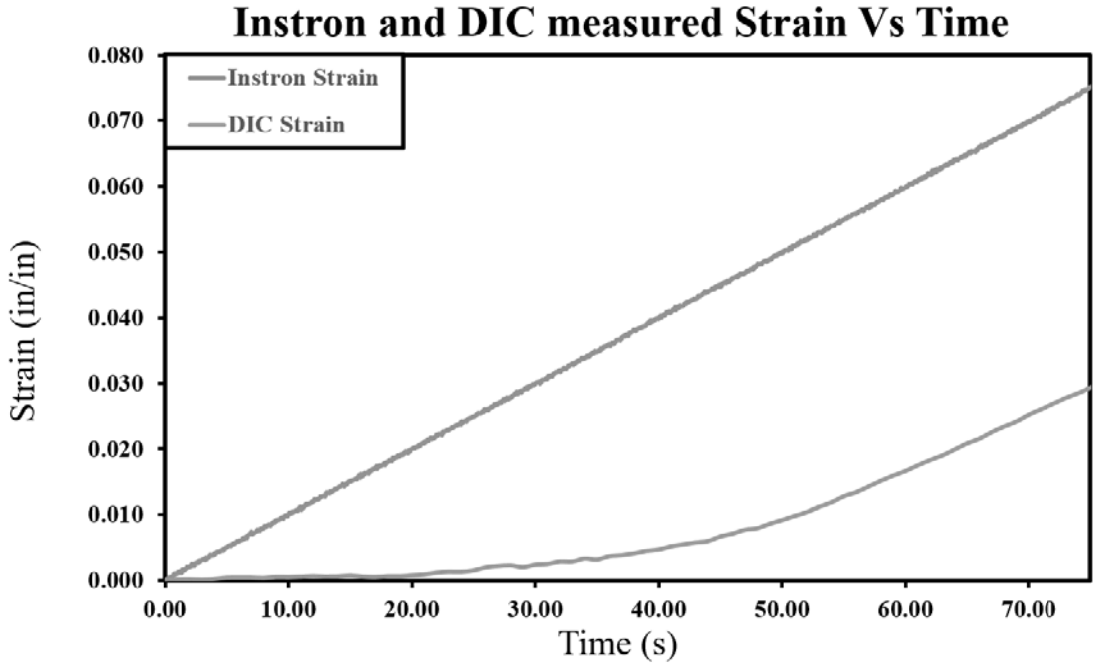

Figure 4.3. During the initial ramp of the load on the sample the Instron measures more strain than the sample experiences

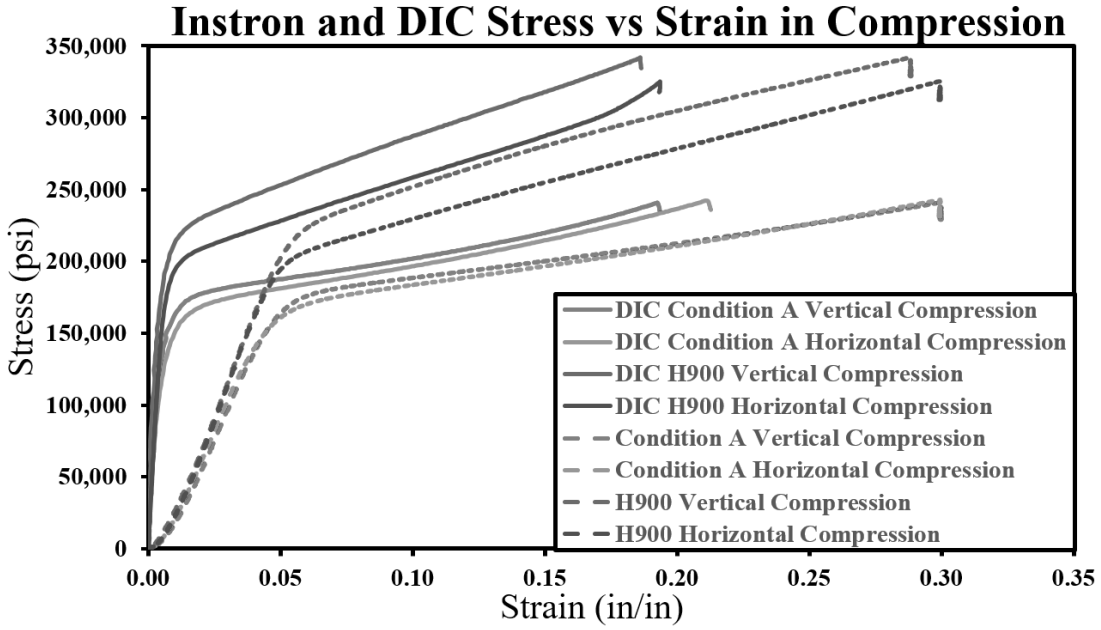

Figure 4.4. Compression stress vs strain curves using the Instron strain data (dashed lines) and the DIC strain data (solid lines)

Table 4.2 shows a comparison of the quasi static compression results. The compression test results show the Condition A vertical specimens are stronger than the wrought material and the Condition A horizontal specimens are slightly weaker. Fr the H900 heat treatment, the vertical specimens have about the same YS as the wrought material and the horizontal specimens are about 9% weaker than the wrought material. Because the values of the wrought material shown are from tension testing it is expected that the compression testing results would be higher. This is due to the compressive forces closing dislocation within the material, effectively causing work hardening of the material during the test. However, for the AM material we do not see a significant increase in the YS except for the Condition A vertical specimens. The elastic modulus is not given for condition A wrought material, but it is significantly lower than the heat treated value presented. For the H900 AM specimens the young's modulus of both the H900 orientations is slightly higher than the wrought material. Again because of the work hardening curring compression the youngs modulus is slightly larger. The Condition A material shows a small amount of anisotropy between the build orientations, the vertical orientation is approximately 5% stronger. This anisotropy is increased significantly by the heat treatment, the vertical orientation is approximately 10% stronger. The H900 heat treatment increases the YS of the horizontal specimens by 30% and the YS of the vertical specimens by 33%.

Heat Treatment	Condition A Horizontal	Condition A Vertical	H900 Horizontal	H900 Vertical
YS increase vs Wrought (%)	-1.114	6.455	-9.103	0.450
E increase vs Wrought (%)	-29.180	-20.945	5.829	5.476
Orientation YS Increase (%)		7.508		10.552
Orientation E Increase (%)		11.628		-0.334
Heat Treatment YS increase (%)			31.922	35.162
Heat Treatment E increase (%)			49.433341	33.4206

Table 4.2. Comparison of Quasi-Static Compression Test Results

True stress vs strain curves are important in understanding how the material reacts as the strain increases beyond the elastic region. As the specimens begin to deform they no longer have the same instantaneous cross sectional area. The engineering stress strain curves do not account for this change and will overestimate the stress and strain that the sample is undergoing. This overestimation will result in false values at increasing strains that will show a material response that can be stiffer or softer than it actually is. By calculating the true stress strain curves we can understand how the material reacts during plastic deformation. Figure 4.5 shows the trues stress vs strain response of the compression. The Condition A specimens for both orientations respond very similarly and they exhibit almost no strain hardening during the initial elastic portion. As the strain increases the curves do start to exhibit strain hardening at a strain of 0.1. This strain hardening is a result of the barreling that occurs in the samples. The barreling of the samples results in an increased cross section. The larger cross section requires a large force for displacement, increasing the amount of stress. The barreling can be accounted for through the use of DIC. DIC can measure the true strain at any point and will account for the effect of barreling. The H900

specimens for both orientations also respond very similarly and they exhibit almost no strain hardening during the initial elastic portion.

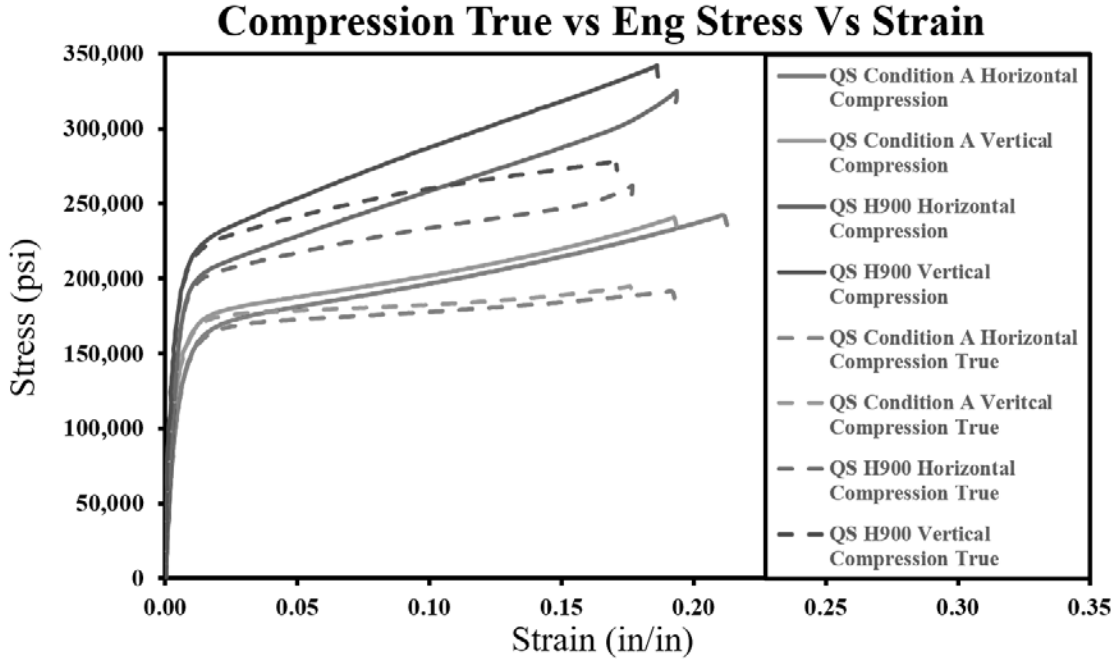

Figure 4.5. True and Engineering stress vs strain curves

4.1.2 Quasi-Static Tension Testing

The results of the quasi-static tension testing are also stress vs strain curves. From these stress vs strain curves, the modulus of Elasticity, YS, and the UTS can be obtained. The stress vs strain curves for the quasi-static tension testing is shown in figure 4.6. Further analysis of the data calculated the modulus of elasticity and the 0.2 % YS using the same method from the compression testing. Further analysis of the data established the modulus of elasticity and the 0.2 % YS as shown in table 4.3.

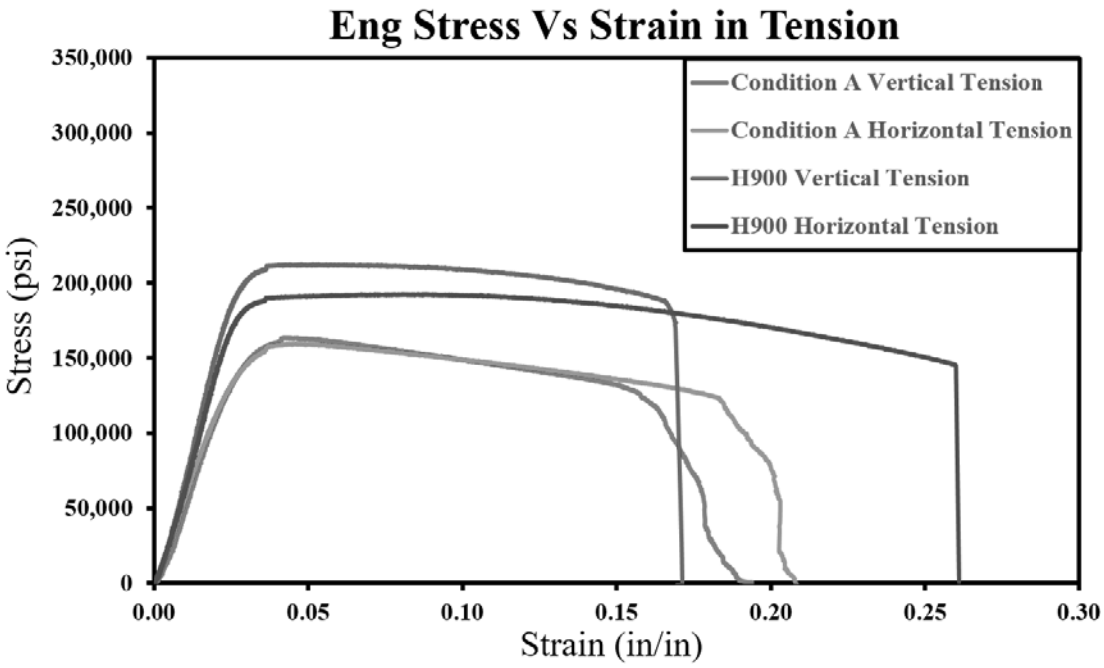

Figure 4.6. Quasi static tension engineering stress vs strain

Specimen	Ultimate Stress (psi)	Yield Stress (psi)	E(Instron) (psi)	E(DIC) (psi)	Failure Strain (in/in)
Condition A H1	161534	130450	6083766	18573795	0.182
Condition A H2	159650	132545	5926599	19682382	0.209
Condition A H3	157462	129163	6070866	18381929	0.192
Condition A H4	159501	132246	5739266	17999323	0.205
Average	159537	131101	5955124	18659357	0.197
Condition A V1	163281	131848	6313766	19296067	0.186
Condition A V2	162187	130058	6351888	20137216	0.162
Condition A V3	163380	130605	6581766	20605576	0.194
Condition A V4	162038	131649	6466099	19420775	0.193
Average	162721	131040	6428380	19864909	0.184
H900 H1	193730	177960	7803855	27763188	0.224
H900 H2	192824	177356	7518400	29405024	0.244
H900 H3	190735	178301	7318033	26671252	0.249
H900 H4	190735	178102	7562366	29749600	0.253
Average	192006	177930	7550664	28397266	0.243
H900 V1	211375	189491	8150233	27570596	0.141
H900 V2	212380	189737	8544000	29798316	0.179
H900 V3	211723	191910	8433499	28992956	0.135
H900 V4	212481	190343	8613700	28641904	0.153
Average	211990	190370	8435358	28750943	0.152
AK Steel Condition A	161000	140000	28500000	N/A	0.084
AK Steel H900	209000	201000	28500000	N/A	0.101

Table 4.3. Quasi static tension results

The results from the tension data also revealed that the modulus of elasticity was significantly lower than expected, approximately one quarter of the expected value which led to further analysis of the strain. All the tension tests were accomplished with DIC. The strain vs time plots for the tension test showed similar results to the compression as shown in figure 4.7. The tension data shows a significant increase in strain at 112 seconds, as shown in figure 4.8. This is caused by the increase in strain rate after the sample surpasses its yield strength. As with the compression specimens, the gauge section of the test specimen is small at only 0.250 in. The relatively small amount of compliance deformation from the Instron results in a significant increase in the strain measured by the Instron. This increase in the strain again results in the slope of the stress vs strain curve to be significantly reduced. Using the strain calculated from the DIC the modulus of elasticity is significantly higher. In table 4.1 the E(Instron) refers to the modulus of elasticity calculated using the Instron strain, and E(DIC) refers to the modulus of elasticity calculated using the DIC strain. This effect can be seen in figure 4.9 in which the solid stress vs strain curves are calculated using the DIC strain and the dashed curves are the stress vs strain curves for the Instron.

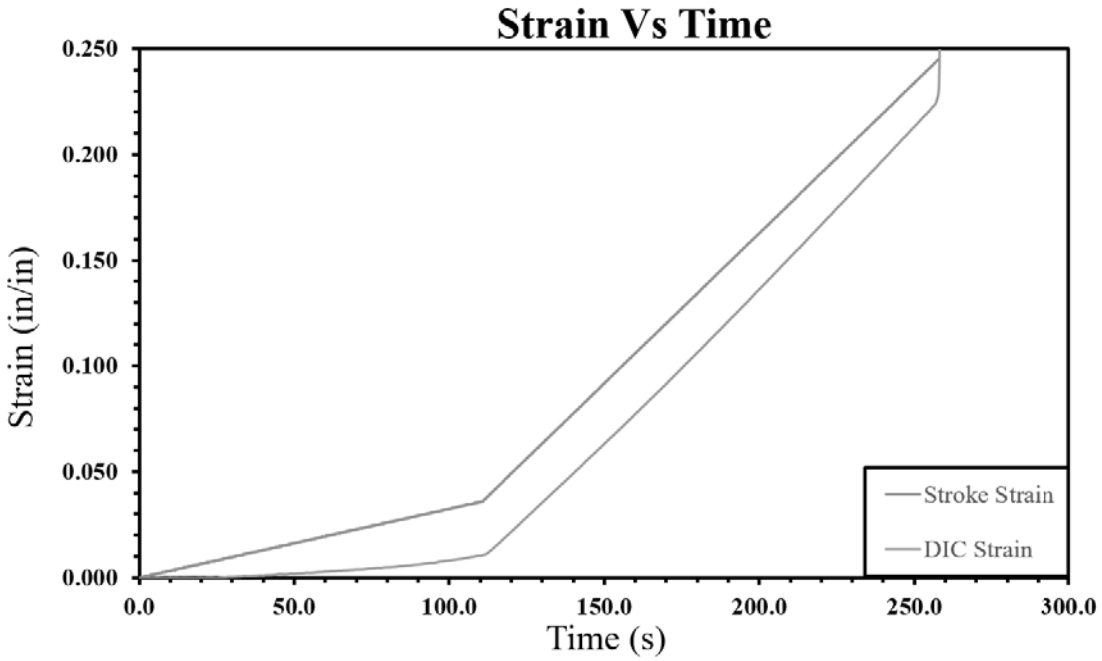

Figure 4.7. Tension Instron strain and DIC strain vs time

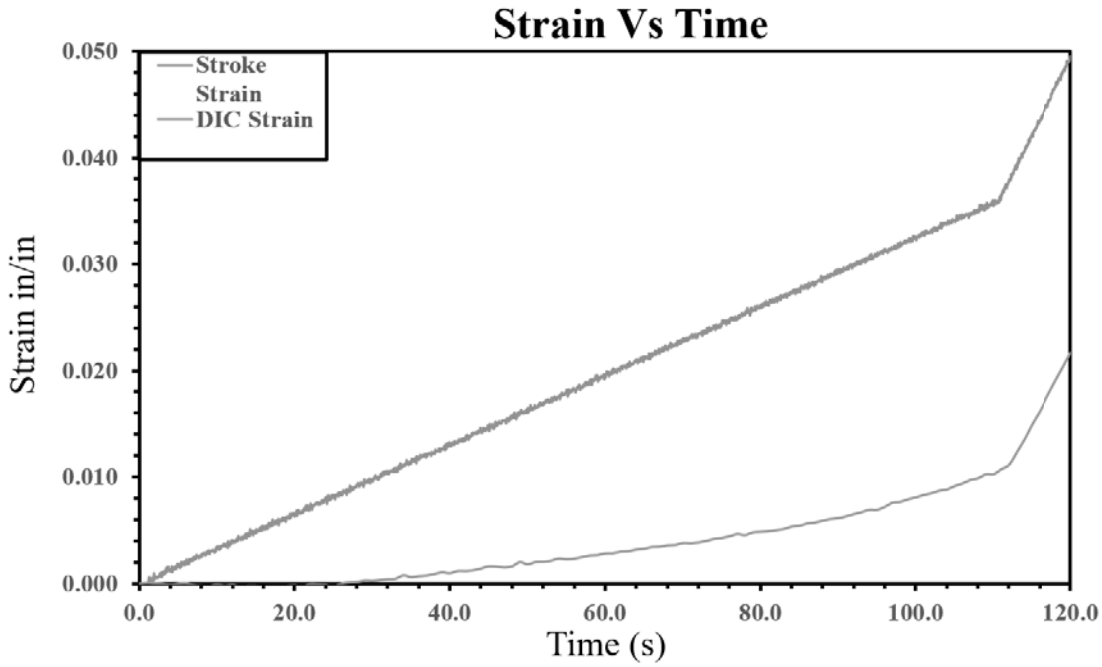

Figure 4.8. Tension Instron strain and DIC strain vs time

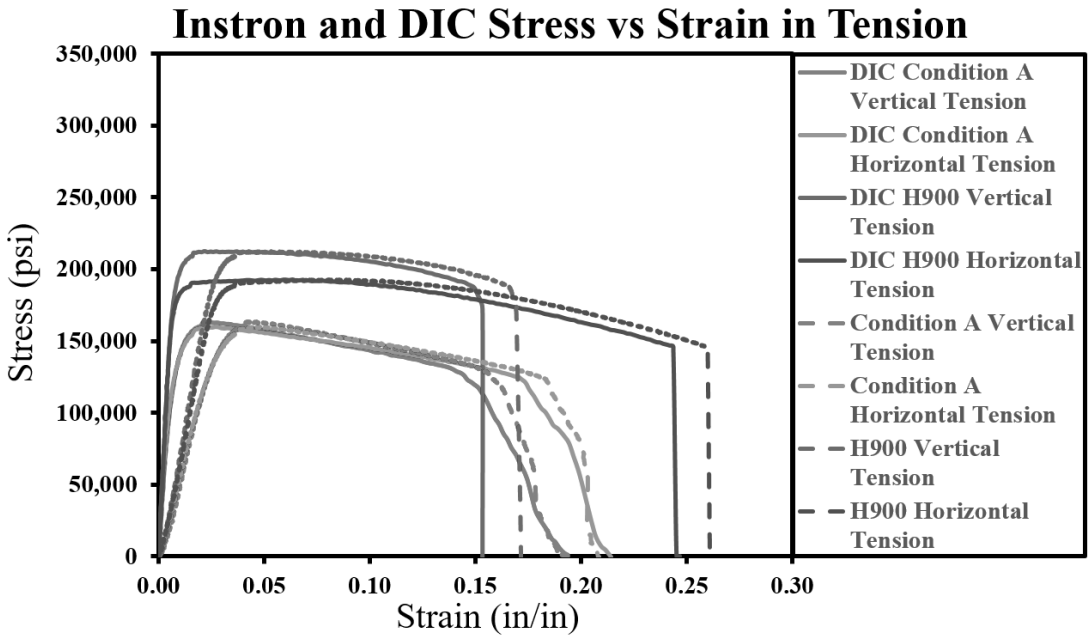

Figure 4.9. Tension stress vs strain curves using the Instron strain data (dashed lines) and the DIC strain data (solid lines)

Table 4.4 shows a comparison of the quasi static tension results. The tension tests show the YS of the both the Condition A orientations to be weaker than the wrought material. The UTS however, is only about 1% different with the horizontal orientation being weaker and the vertical orientation being stronger. The YS of the H900 specimens is also significantly lower, with the horizontal orientation showing a more significant decrease. The H900 vertical UTS is very close to the wrought material, but the horizontal orientation UTS lower. The values of the AK Steel should be comparable since they are from tension testing. The Condition A material shows almost no anisotropy between the build orientations for both the YS and only and UTS. The anisotropy appears after the material under goes the H900 Heat treatment. at the H900 heat treatment the vertical orientation has a higher YS and UTS. As expected the H900 heat treatment increases the YS of the vertical specimens by 45% and the UTS of the vertical specimens by 35% which is identical to the wrought material. The Horizontal specimens, however, don't increase as much with only a 35%

increase in YS and 20% increase in the UTS. The elastic modulus of both the H900 orientations is within 1% of the wrought material with the Condition A orientations significantly lower. One of the areas where the AM material is significantly different from the wrought material is the FS. It is difficult to compare the failure strain values to the wrought material values due to the differences in geometry of the test specimens. Typically with the increase in YS the FS decreases, but the horizontal orientation shows an increase in both. The FS does show anisotropic properties for the AM material. The Condition A horizontal specimens have a slightly higher FS over the vertical orientations but at the H900 heat treatment the horizontal specimens are significantly higher, over 37%.

Heat Treatment	Condition A Horizontal	Condition A Vertical	H900 Horizontal	H900 Vertical
YS vs Wrought (%)	-6.356	-6.400	-11.478	-5.289
UTS vs Wrought (%)	-0.909	1.069	-8.131	1.431
E vs Wrought (%)	-34.529	-30.299	-0.360	0.881
Orientation YS Increase (%)		-0.047		6.992
Orientation UTS Increase (%)		1.996		10.408
Orientation FS Increase (%)		-6.743		-37.333
Orientation E Increase (%)		6.461		1.245
Heat Treatment YS increase (%)			35.720	45.276
Heat Treatment UTS increase (%)			20.352	30.278
Heat Treatment FS increase (%)			23.170	-17.231
Heat Treatment E increase (%)			52.188	44.732

Table 4.4. Comparison of Quasi static tension results

Trues stress vs strain curves for tension testing are very important for understanding if the material hardens or softens in the plastic regime. Figure 4.10 shows both the engineering and true stress vs strain response for the tension testing. Through the use of DIC the true strain can be measured throughout the test. DIC creates a ful field measurement and is able to calculate the exact strain of the material at any point. The response for both Condition A orientations is very similar. Both exhibit strain hardening throughout the testing until the material starts to fail. The true stress strain curves for both of the H900 orientations also react very similarly. Again, both orientations exhibit strain hardening until they reach the point of failure.

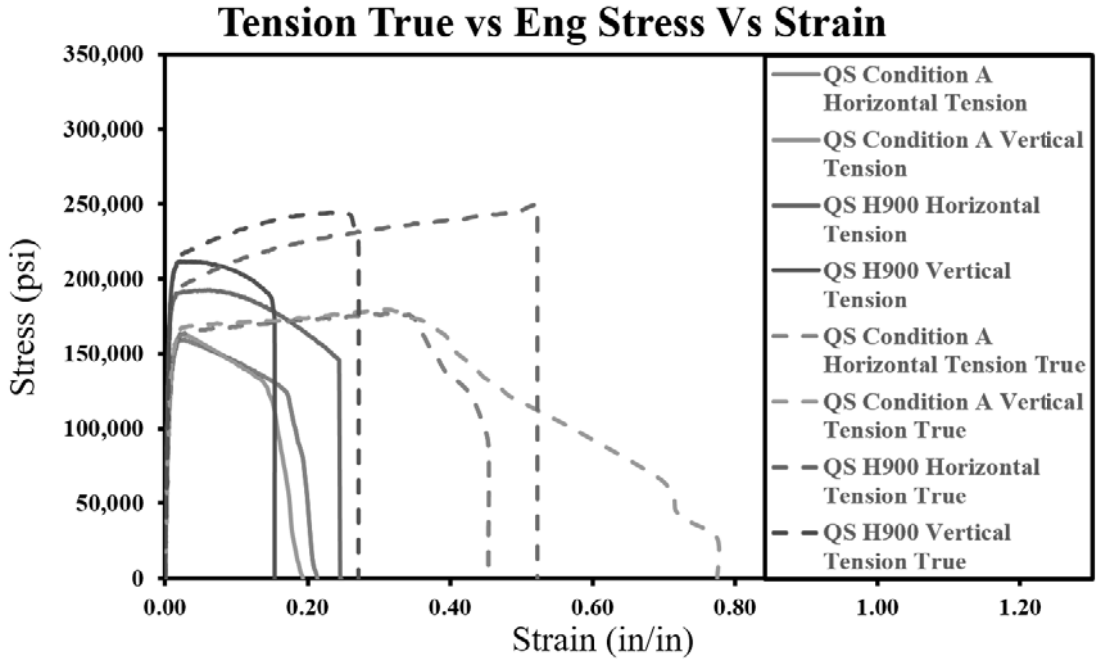

Figure 4.10. True and Engineering stress vs strain curves for the Horizontal orientation

4.2 Split Hopkinson Pressure Bar Compression and Tension Testing

SHPB compression testing was conducted at each of the eight metallurgical condition. The SHPB tension testing was conducted at twelve metallurgical conditions. The SHPB testing is conducted to analyze the effect that strain rate has on the

strength of material. This testing will also reveal any effects the build orientation and heat treatment have on the strength of the material, and if they interact with the strain rate. At each compression test point 3 specimens were tested to verify the repeatability of each test and identify any potential outliers.

4.2.1 Split Hopkinson Pressure Bar Compression Testing

The results of the SHPB compression testing are similar to the quasi static testing, stress vs strain curves. SHPB testing, however, also results in strain rate and force vs time. From these stress vs strain curves, the YS and young's modulus can be determined. In addition to the stress vs strain curves the strain rate can also be determined. Testing was conducted at a low strain rate, 500 s^{-1}, and high strain rate, 800 s^{-1}. Figure 4.16 shows both the low and high rate stress vs strain curves. The strain rate is calculated as the average strain rate after the desired strain rate is reached.

The machining of the SHPB samples used a wire cutter to cut the samples to length. The effect of using the wire cutter to cut the samples resulted in slightly uneven ends of the samples. During the test as the force from the incident bar is applied to the sample the slightly longer ends start to compress first. The edges compress until the surface is flat and the entire sample is engaged. Once the entire sample face is engaged, the stress is evenly distributed across the sample. This results in an increased amount of strain during the initial samples compression. The effect of this increased strain is a reduction in the slope of the stress vs strain curve, the young's modulus. Because this only occurs during the initial portion of the testing, the young's modulus is invalid, but the yield stress and the plasticity data are correct.

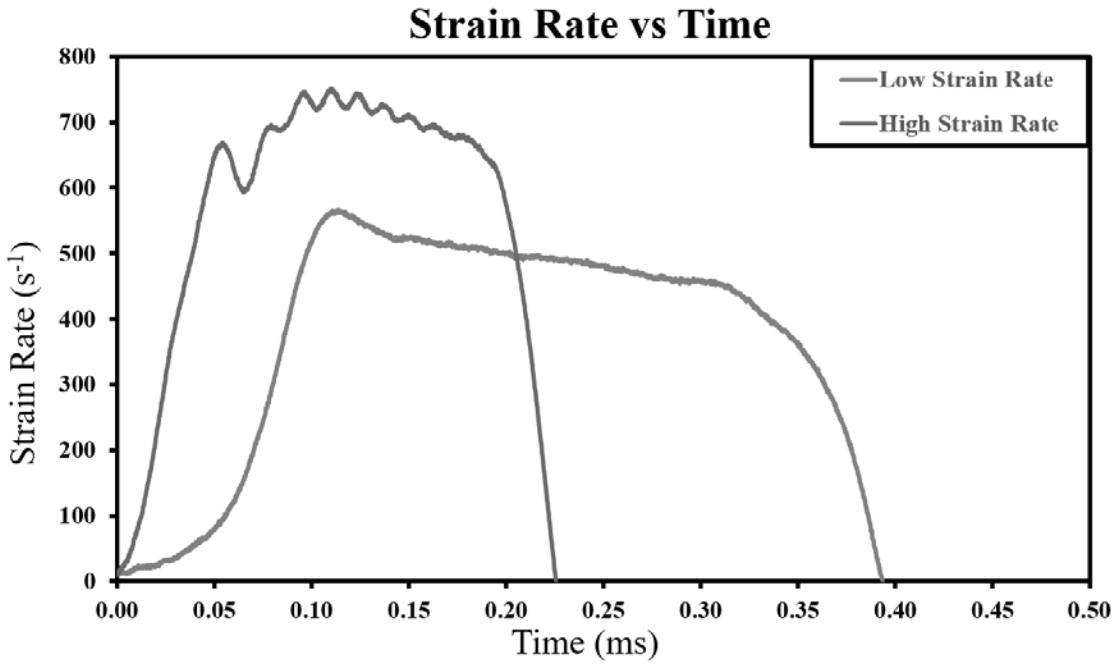

Figure 4.11. Low rate (500 s^{-1}) and high rate (800 s^{-1}) strain rate vs time for the Condition A horizontal SHPB compression tests

4.2.1.1 Low Rate Split Hopkinson Pressure Bar Compression Testing

The low strain rate testing was conducted at 500 s^{-1}. The stress vs strain curves for the low rate compression testing are shown in figure 4.12. Further analysis of the data establishes the low strain rate 0.2 % YS as shown in table 4.5.

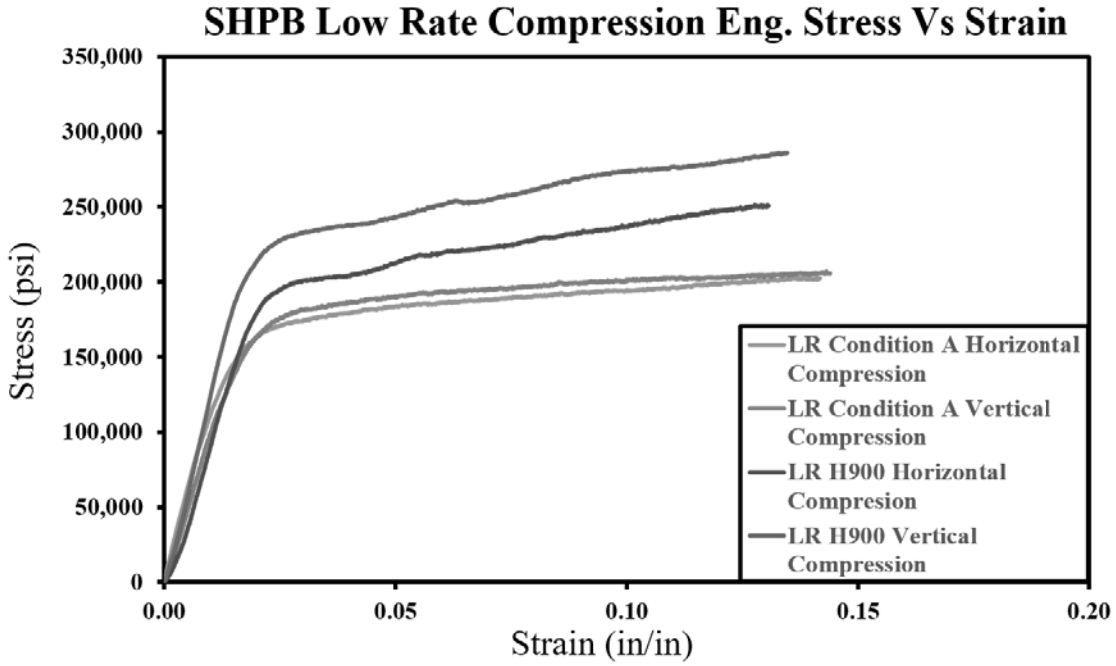

Figure 4.12. SHPB low rate, 500 s^{-1}, compression engineering stress vs strain

Condition	Orientation	Strain Rate (1/s)	Yield Stress (psi)
Condition A	Horizontal	483	143883
Condition A	Horizontal	426	142024
Condition A	Horizontal	477	140152
Average	Horizontal	462	142020
Condition A	Vertical	593	153653
Condition A	Vertical	431	149447
Condition A	Vertical	511	150259
Average	Vertical	512	151120
H900	Horizontal	465	179325
H900	Horizontal	444	180297
H900	Horizontal	464	179630
Average	Horizontal	458	179751
H900	Vertical	506	207926
H900	Vertical	527	200443
H900	Vertical	500	205345
Average	Vertical	511	204571
AK Steel Condition A	N/A	N/A	140000
AK Steel H900	N/A	N/A	201000

Table 4.5. Low rate (500 s^{-1}) SHPB compression results

A comparison of the results from the low rate testing are shown in table4.7. The results of this testing at Condition A show a almost no increase in the YS for the horizontal specimens with a slight increase in the YS of the vertical specimens . The H900 horizontal specimen shows significantly lower YS while the vertical specimen is very comparable. Because the values of the wrought material shown are from tension testing, the results from compression testing should be higher due to the compressive forces closing dislocation within the material, effectively causing work hardening of the material. However during the low rate testing, the AM material does not exhibit a significant increase in the yield stress except for the Condition A vertical orientation. The Condition A material shows a small amount of anisotropy between the build orientations, with the vertical orientation having a higher YS than the horizontal orientation. This anisotropy is almost doubled by the heat treatment, with the vertical orientation having a 14% higher YS. The H900 heat treatment increases the YS of the horizontal specimens by 27% and the YS of the vertical specimens by 35%, both of which are lower than the expected 45% increase shown by the wrought material in quasi-static testing.

Heat Treatment	Condition A Horizontal	Condition A Vertical	H900 Horizontal	H900 Vertical
YS vs Wrought (%)	1.443	7.942619048	-10.572	1.777
Orientation YS Increase (%)		6.408		13.808
Heat Treatment YS increase (%)			26.567	35.370

Table 4.6. Comparison of the low rate (500 s^{-1}) SHPB compression results

The true stress vs strain curves were calculated for the low rate compression tests and are shown in Figure 4.13. This plot shows how the AM material reacts in the plastic regime at the low strain rate and whether the material exhibits strain hardening or softening. The Condition A specimens exhibits almost no strain hardening for both orientations. The H900 specimens show some minor strain hardening. The reaction

at this strain rate is almost identical to the QS results for the strain hardening.

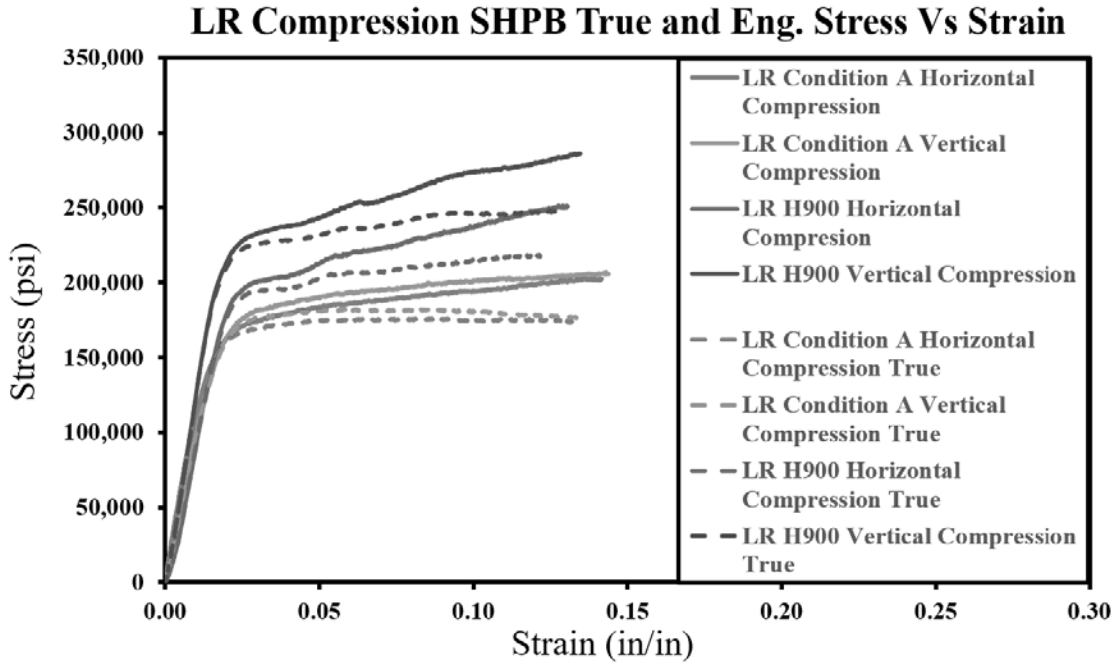

Figure 4.13. Low rate, 500 s^{-1}, SHPB compression engineering (solid lines) and true (dashed lines) stress vs strain curves

4.2.1.2 High Rate Split Hopkinson Pressure Bar Compression Testing

The high strain rate testing was conducted at the same test conditions as the low rate, but at 800 s^{-1}. Figure 4.14 shows the high rate stress vs strain curves and table 4.7 shows the results from the testing.

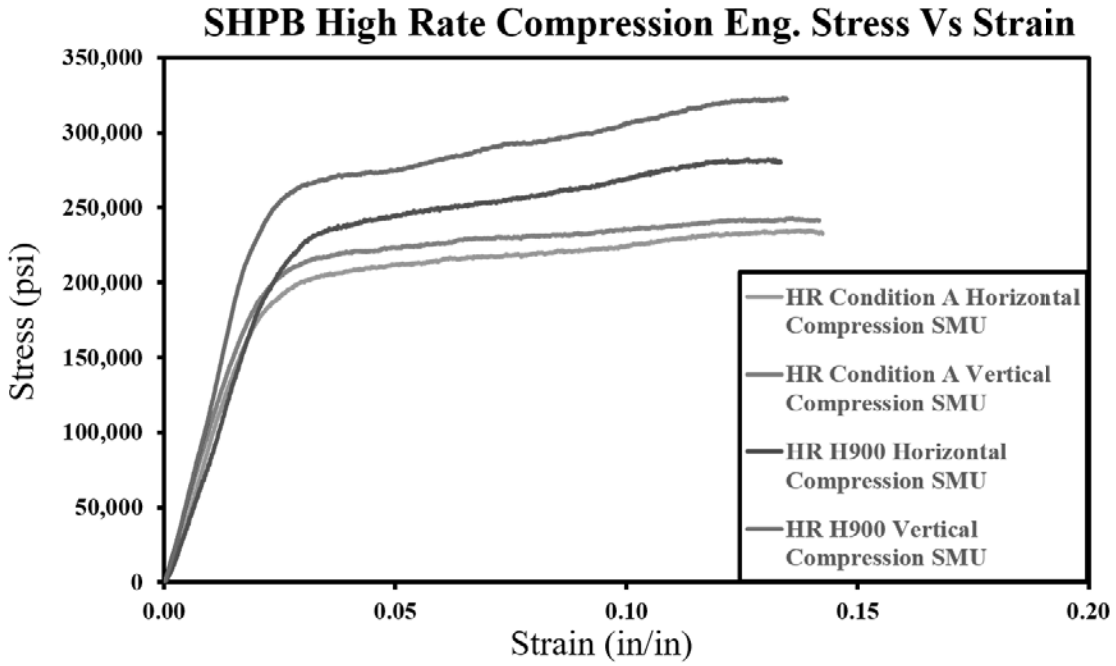

Figure 4.14. SHPB high rate, 800 s^{-1}, compression engineering stress vs strain

Condition	Orientation	Strain Rate (1/s)	Yield Stress (psi)
Condition A	Horizontal	801	171101
Condition A	Horizontal	808	173872
Condition A	Horizontal	808	173132
Average	Horizontal	806	172702
Condition A	Vertical	861	187012
Condition A	Vertical	806	189550
Condition A	Vertical	813	183314
Average	Vertical	827	186625
H900	Horizontal	693	200907
H900	Horizontal	756	209551
H900	Horizontal	762	201777
Average	Horizontal	737	204078
H900	Vertical	790	237587
H900	Vertical	799	235310
H900	Vertical	784	240720
Average	Vertical	791	237872
AK Steel Condition A	N/A	N/A	140000
AK Steel H900	N/A	N/A	201000

Table 4.7. High rate (800 s^{-1}) SHPB compression results

A comparison of the results from the low rate testing is shown in table4.8. The high rate compression tests show a significant increase in the YS of all the specimens, with the exception of the H900 horizontal specimens over the wrought material. The largest increase in the yield strength is by the Condition A samples with the vertical experiencing a greater increase. Both heat treatments show anisotropic behavior with the vertical orientation being stronger than the horizontal. Condition A experiencing an 8% difference in YS with the H900 heat treatment exhibiting a much larger increase of 17%.

Heat Treatment	Condition A Horizontal	Condition A Vertical	H900 Horizontal	H900 Vertical
YS vs Wrought (%)	23.358	33.304	1.532	18.344
Orientation YS Increase (%)		8.062		16.559
Heat Treatment YS increase (%)			18.168	27.460

Table 4.8. Comparison of high rate (800 s^{-1}) SHPB compression results

The true stress vs strain curves were calculated for the high rate compression tests and are shown in Figure 4.15. This plot shows how the AM material reacts in the plastic regime at the high strain rate and whether the material exhibits strain hardening or softening. The Condition A specimens exhibits almost no strain hardening whereas the H900 does show some minor strain hardening. The strain hardening characteristics at this strain rate is very similar to both the quasi static testing and the low rate testing.

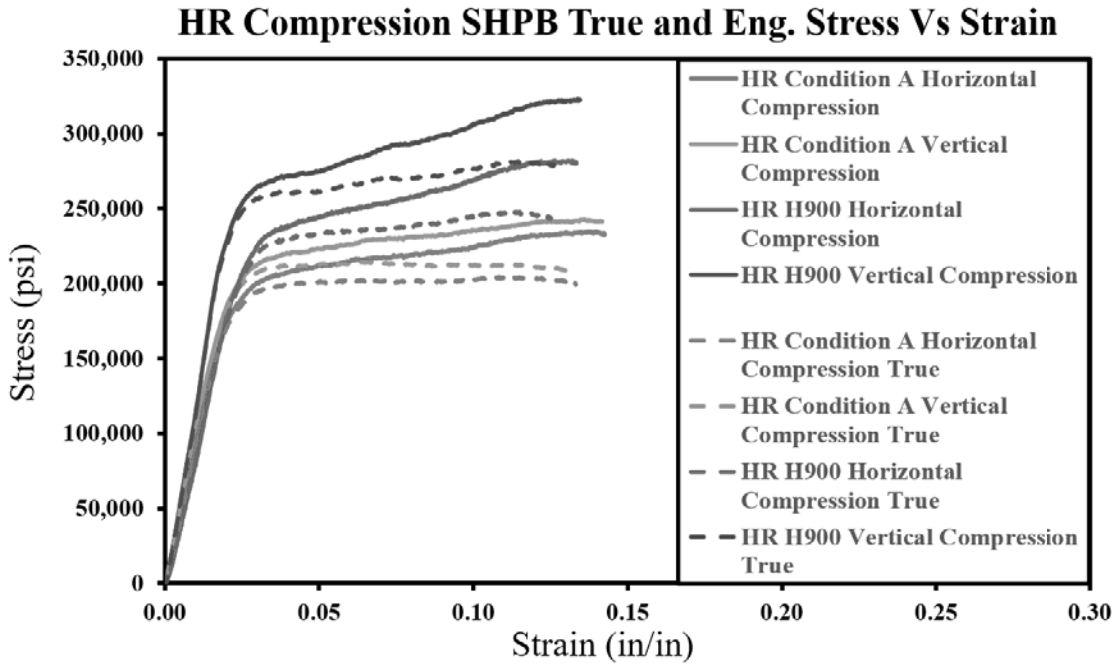

Figure 4.15. High rate, 800 s^{-1}, SHPB compression engineering (solid lines) and true (dashed lines) stress vs strain curves

The low rate and high rate stress vs strain curves are plotted together in figure 4.16. This figure shows how the increased strain rate increases the strength of the material in compression. There is a trend in the compression testing that with the increasing YS from the higher strain rate, the anisotropy between the orientations increase.

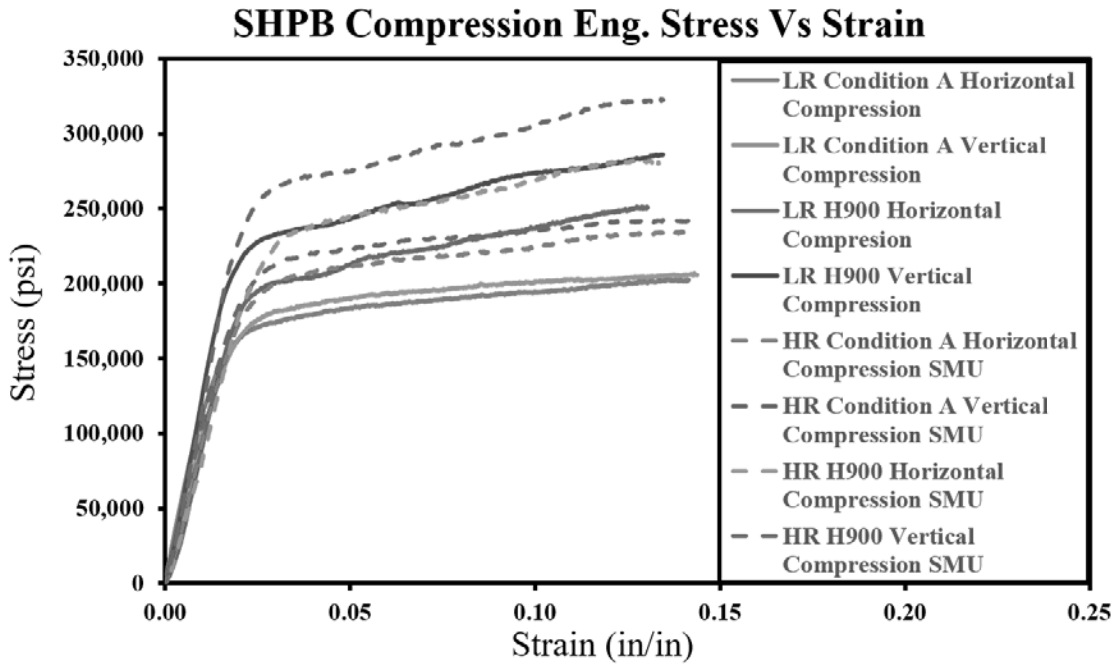

Figure 4.16. Low rate, 500 s^{-1} (solid lines), and high rate, 800 s^{-1} (dashed lines), SHPB compression engineering stress vs strain curves

4.2.2 Split Hopkinson Pressure Bar Tension Testing

The results of the SHPB tension testing given below are from testing that was conducted by Allison Dempsey[17]. The results from the tension testing are the same as from the SHPB compression testing. From the tension testing, we can also get the UTS. Tension testing was also conducted at a low strain rate, 500 s^{-1}, and high strain rate, 800 s^{-1}. Figure 4.23 shows both the low and high rate stress vs strain curves for the As Built and H900 specimens. Figure 4.24 shows both the low and high rate stress vs strain curves for the H1025 specimens. Further analysis of the data establishes the UTS. Because of the length of the tension samples it takes a longer time for the stress to build up and achieve equilibrium in the sample. For the tension testing it was determined the elastic response occurred during the stress equilibrium phase and therefore the modulus and yield stress are not accurate. The initial hump in all of the tension graphs is an artifact of the specimen achieving equilibrium.

4.2.2.1 Low Rate Split Hopkinson Pressure Bar Tension Testing

The low strain rate testing was conducted at 500 s^{-1}. The stress vs strain curves for the low rate tension testing is shown in figure 4.17. The results of the tests are shown in table 4.9.

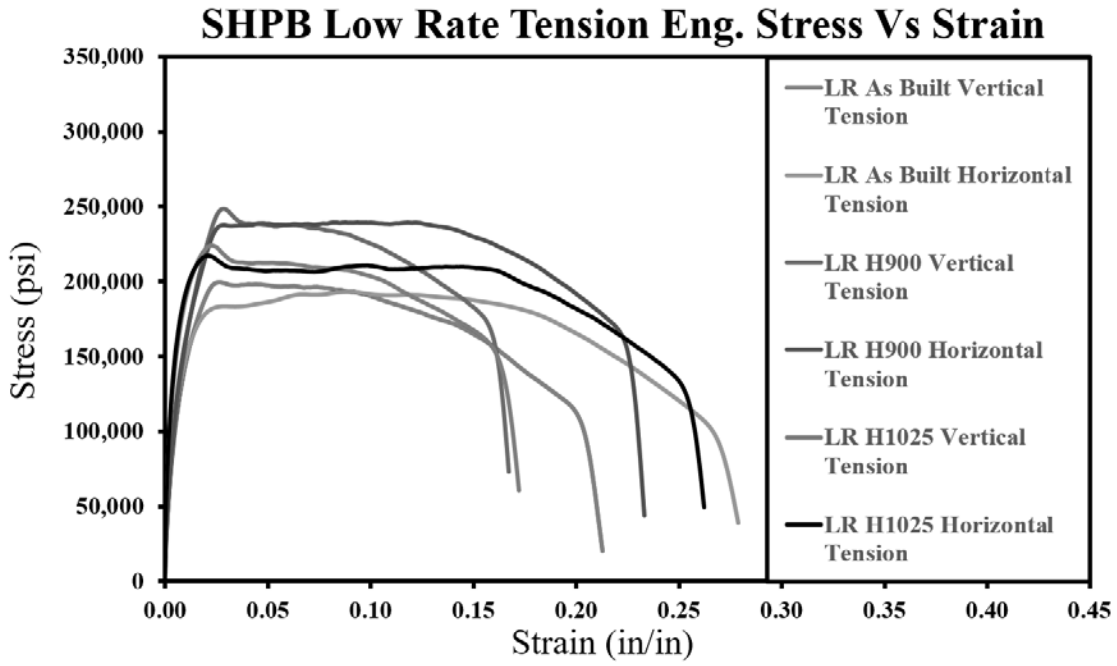

Figure 4.17. SHPB Low Rate, 500 s^{-1}, Tension Engineering Stress vs Strain

Condition	Specimen	Strain Rate (1/s)	Ultimate Stress (psi)	Failure Strain
As Built	Horizontal	500	193242	0.279
As Built	Horizontal	470	195808	0.290
Average	Horizontal	485	194525	0.285
As Built	Vertical	460	199692	0.213
Average	Vertical	460	199692	0.213
H900	Horizontal	425	239569	0.233
H900	Horizontal	460	239996	0.230
Average	Horizontal	443	239783	0.232
H900	Vertical	485	248406	0.167
H900	Vertical	470	246864	0.176
Average	Vertical	478	247635	0.172
H1025	Horizontal	495	218143	0.269
H1025	Horizontal	500	217083	0.249
Average	Horizontal	498	217613	0.259
H1025	Vertical	520	224034	0.177
H1025	Vertical	515	220894	0.173
Average	Vertical	518	222464	0.175
AK Steel Condition A	N/A	N/A	161000	0.084
AK Steel H900	N/A	N/A	209000	0.101
AK Steel H1025	N/A	N/A	174000	0.122

Table 4.9. Low rate SHPB tension results

The Comparison of the low rate tension tests is shown in table 4.11. The UTS of both orientations of the As Built specimens is significantly higher than the wrought material. The H900 orientations also show a significant increase in UTS, however the increase is not as large as the As Built. Both orientations of the H1025 specimens show the largest increase in UTS, over 25% for both. The build orientation appears to have a small effect on the UTS but a significant effect on the FS. The vertical orientation UTS is slightly stronger for all heat treatments, with the H900 heat treatment experiencing the largest increase. The failures strain is at least 25% lower for all of the vertical orientations with the H1025 heat treatment experiencing the largest reduction. The heat treatment increases the UTS of the H900 specimens for both orientations by about 24% with a corresponding reduction in FS of about

19%. Both orientations of the H1025 samples increase there UTS by a little over 11% but also exhibit a reduction in FS.

Heat Treatment	As Built Horizontal	As Built Vertical	H900 Horizontal	H900 Vertical	H1025 Horizontal	H1025 Vertical
UTS vs Wrought (%)	20.823	24.032	14.728	18.486	25.065	27.853
Orientation UTS Increase (%)		2.656		3.275		2.229
OrientationFS Increase (%)		-25.132		-25.918		-32.432
Heat Treatment UTS increase (%)			23.266	24.008	11.869	11.404
Heat Treatment FS increase (%)			-18.629	-19.484	-8.963	-17.840

Table 4.10. Low rate SHPB tension results comparison

The true stress vs strain curves were calculated for the low rate tension tests and are shown in Figure 4.18 and 4.19 . These plots shows how the AM material reacts in the plastic regime at the low strain rate and whether the material exhibits strain hardening or softening. The true stress vs strain graphs were calculated using a Bridgman correction factor. The initial hump in the graphs is due to the sample still achieving stress equilibrium and makes it difficult to accurately correct for the true stress vs strain. The results of the true stress vs strain show strain softening across the orientations and heat treatments.

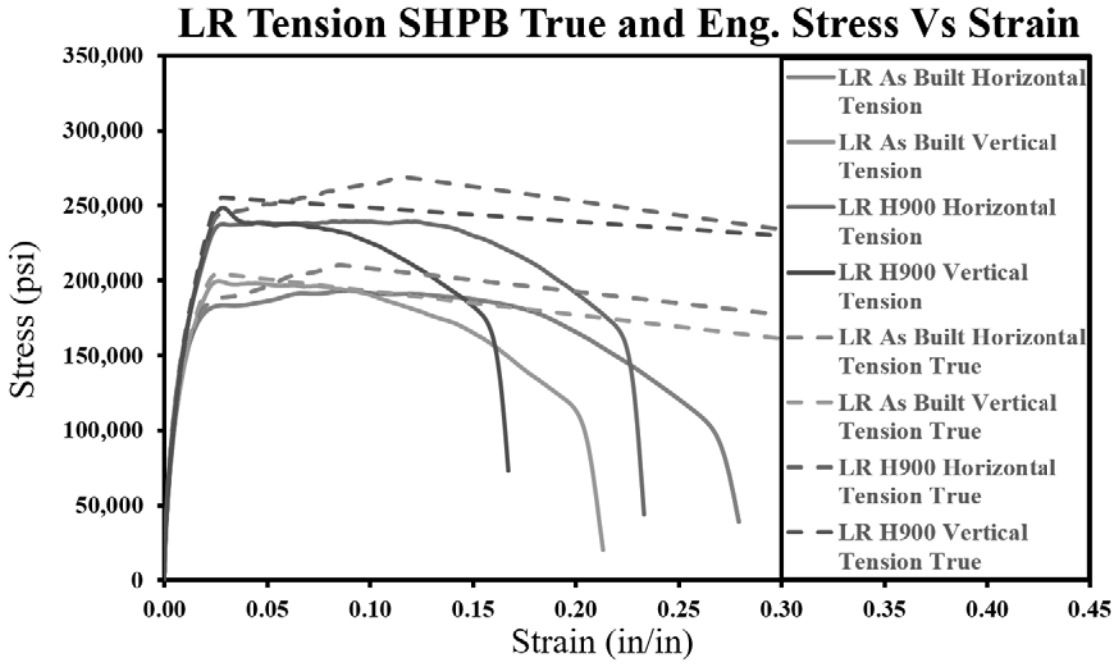

Figure 4.18. SHPB high rate, 800 s^{-1}, tension engineering stress vs strain

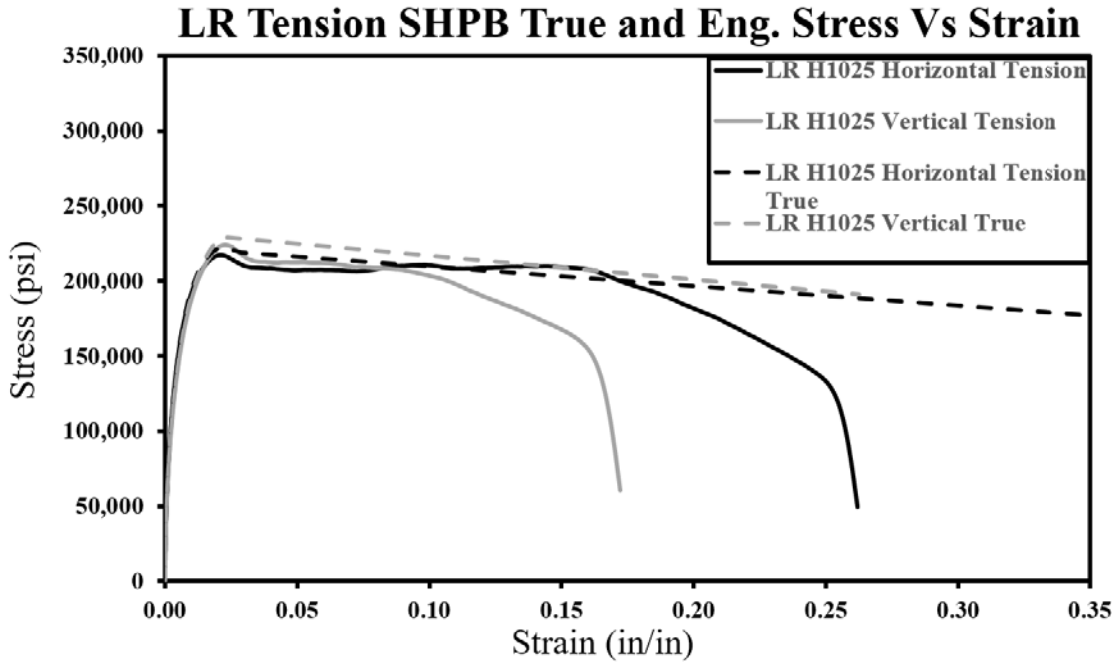

Figure 4.19. SHPB high rate, 800 s^{-1}, tension engineering stress vs strain

4.2.2.2 High Rate Split Hopkinson Pressure Bar Tension Testing

The high strain rate testing was conducted at the same test conditions as the low rate, but at a higher strain rate of 800 s^{-1}. Figure 4.20 shows the high rate stress vs strain curves and table 4.11 shows the results from the testing.

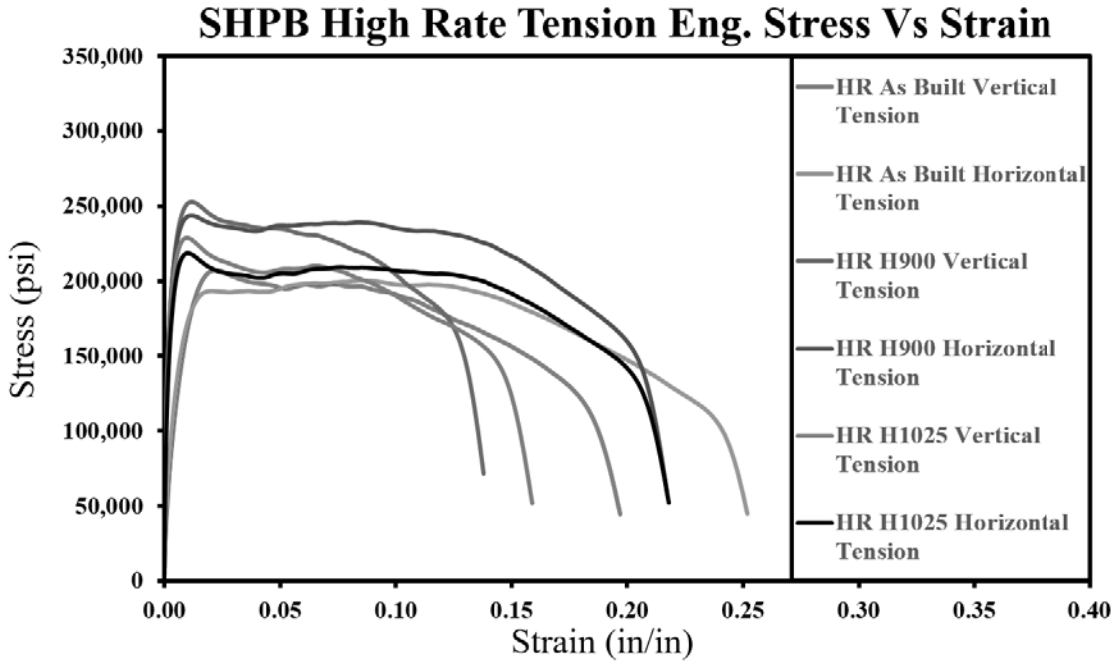

Figure 4.20. SHPB high rate, 800 s^{-1}, tension engineering stress vs strain

Condition	Specimen	Strain Rate (1/s)	Ultimate Stress (psi)	Failure Strain
As Built	Horizontal	740	200084	0.252
As Built	Horizontal	850	195008	0.307
Average	Horizontal	795	197546	0.280
As Built	Vertical	900	207218	0.197
As Built	Vertical	875	206732	0.198
Average	Vertical	888	206975	0.198
H900	Horizontal	790	240413	0.224
H900	Horizontal	825	243835	0.217
Average	Horizontal	808	242124	0.221
H900	Vertical	825	252964	0.138
H900	Vertical	775	252314	0.152
Average	Vertical	800	252639	0.145
H1025	Horizontal	850	224034	0.218
H1025	Horizontal	830	224214	0.210
Average	Horizontal	840	224124	0.214
H1025	Vertical	860	231170	0.158
H1025	Vertical	870	229037	0.159
Average	Vertical	865	230104	0.159
AK Steel Condition A	N/A	N/A	161000	0.084
AK Steel H900	N/A	N/A	209000	0.101
AK Steel H1025	N/A	N/A	174000	0.122

Table 4.11. High rate SHPB tension results

A comparison of the results of the high rate tension testing is shown in table 4.12. The UTS strength of all heat treatments and build orientations is significantly increased at the high strain rate as well. The H1025 heat treatment shows the largest increase in UTS. The H900 exhibits the lowest increase in UTS. As has been seen at other test points the vertical specimens show a larger increase in UTS than the horizontal, but experience a lower increase in FS. The build orientation continues to have an effect on the UTS and FS even at the higher strain rate. The vertical orientations show a small increase in YS of about 4%, slightly lower for the H1025. The impact of the heat treatment on the UTS is still significant, with both orientations showing a similar increase. With the increased UTS we see a similar decrease in the

FS.

Heat Treatment	As Built Horizontal	As Built Vertical	H900 Horizontal	H900 Vertical	H1025 Horizontal	H1025 Vertical
UTS vs Wrought (%)	22.699	28.556	15.849	20.880	28.807	32.243
Orientation UTS Increase (%)		4.773		4.343		2.668
OrientationFS Increase (%)		-29.338		-34.240		-25.935
Heat Treatment UTS increase (%)			22.566	22.063	13.454	11.175
Heat Treatment FS increase (%)			-21.109	-26.582	-23.435	-19.747

Table 4.12. High rate SHPB tension results comparison

The true stress vs strain curves were calculated for the high rate tension tests and are shown in Figure 4.21 and 4.22. This plot shows how the AM material reacts in the plastic regime at the low strain rate and whether the material exhibits strain hardening or softening. The true stress vs strain graphs were calculated using a Bridgman correction factor. The initial hump in the graphs is due to the sample still achieving stress equilibrium and makes it difficult to accurately correct for the true stress vs strain. The results of the true stress vs strain show a small amount of strain softening across the orientations and heat treatments.

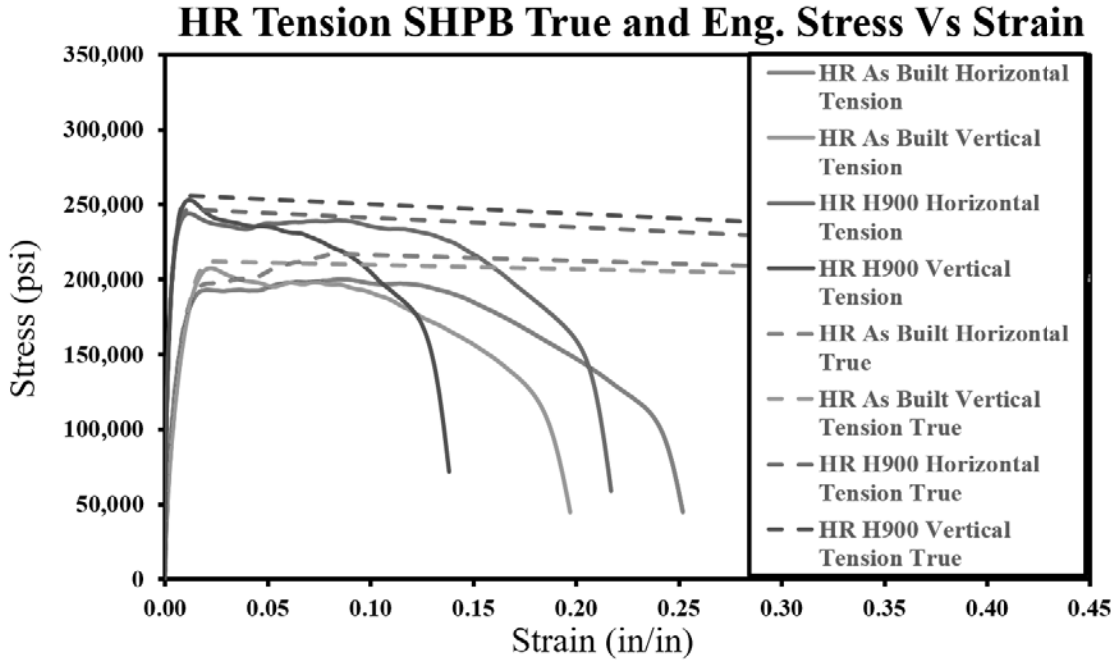

Figure 4.21. Low rate, 500 s^{-1} (solid lines), SHPB tension engineering and true stress vs strain curves for Condition A and H900 heat treatments

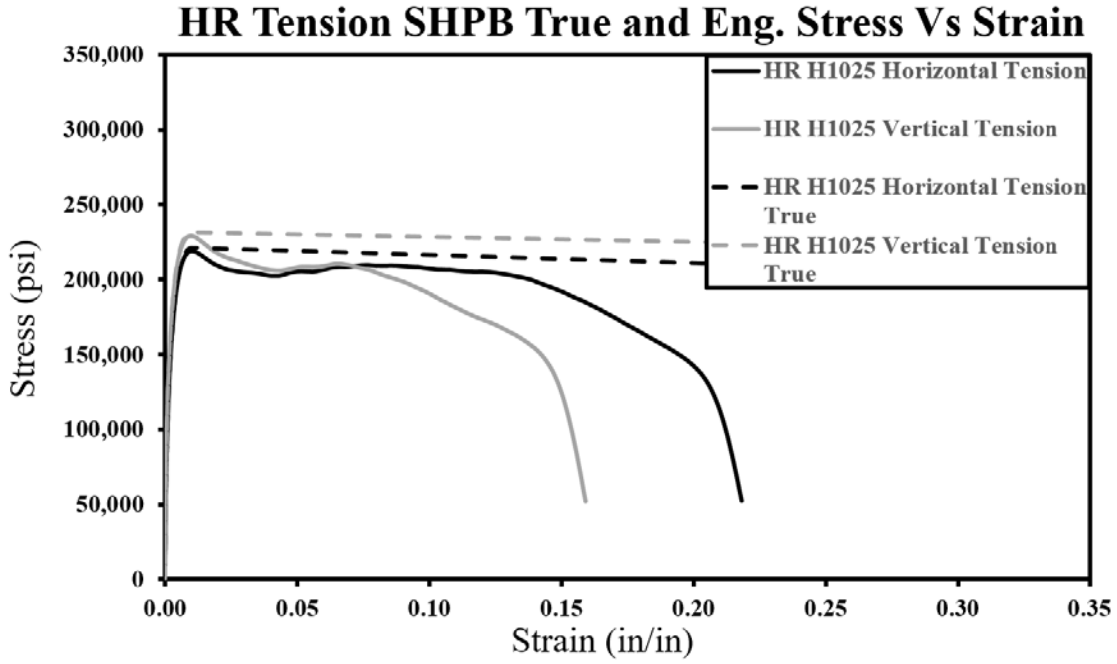

Figure 4.22. Low rate, 500 s^{-1} (solid lines), SHPB tension engineering and true stress vs strain curves for H1025 heat treatments

The low rate and high rate stress vs strain curves are plotted together in figure 4.23 and 4.24. This figure shows how the increased strain rate increases the UTS strength in tension. There is a trend in the tension testing that with the increasing YS from the higher strain rate, the anisotropy between the orientations decreases. It appears that there is a limit to the increase in UTS for all three heat treatments. As both orientations approach this limit the anisotropy is reduced.

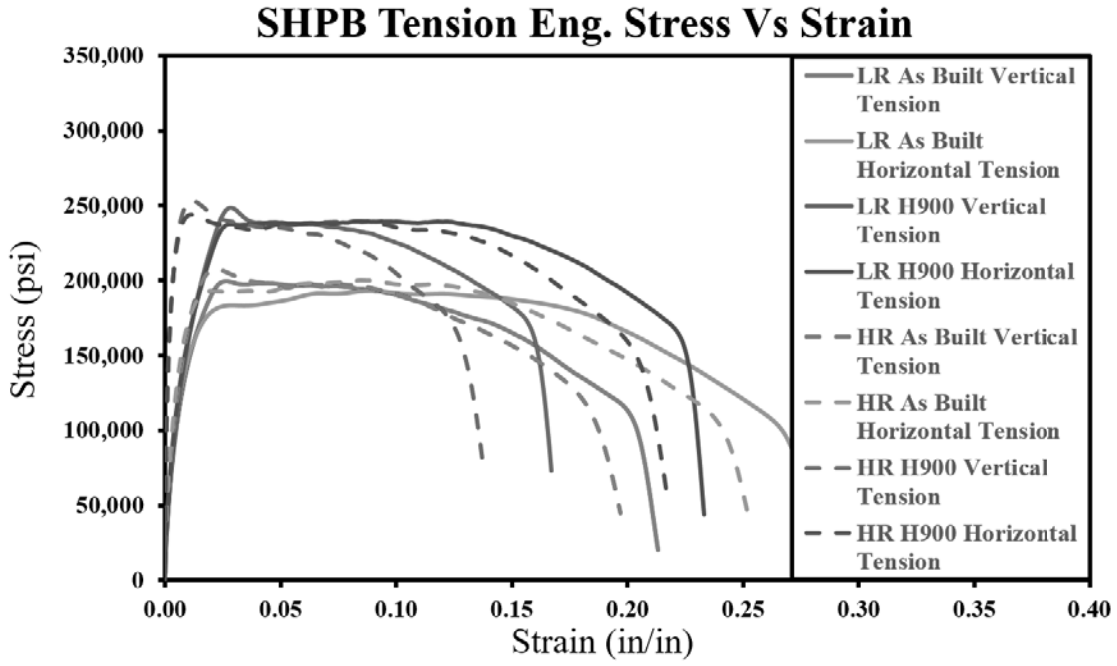

Figure 4.23. Low rate, 500 s^{-1} (solid lines) and High rate, 800 s^{-1} (dashed lines), SHPB tension engineering stress vs strain curves for Condition A and H900 heat treatments

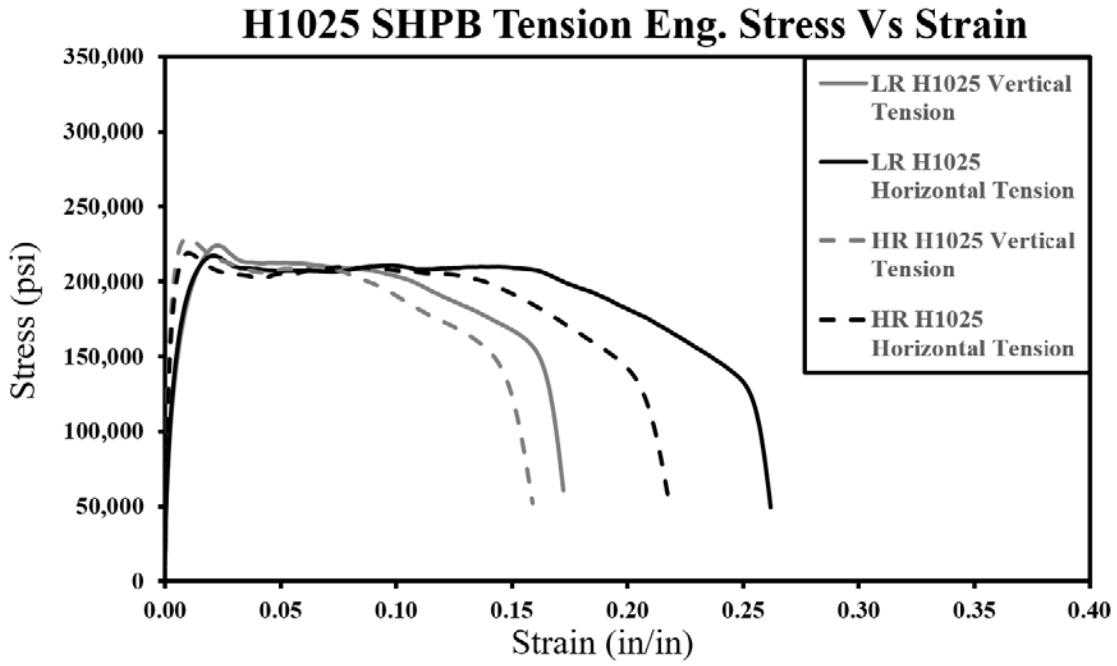

Figure 4.24. Low rate, 500 s^{-1} (solid lines) and High rate, 800 s^{-1} (dashed lines), SHPB tension engineering stress vs strain curves for the H1025 heat treatment

4.3 Microstructural and Compositional analysis

4.3.1 Optical Microscope

Optical microscopy was performed to analyze the effects the DMLS process may have on the material. The macro structure feature of specific interest was the size and shape of the melt pool. Figure 4.25 shows the macro structure of AM built material both in the build plane and perpendicular to the build plane. Individual melt pools were outlined in order to make them more visible. The size of the melt pool was analyzed using the line cut method to determine the average depth and width of the melt pool. The results of the melt pool analysis is shown in table 4.13. The results of this analysis show that the width of the melt pool is larger then the depth.

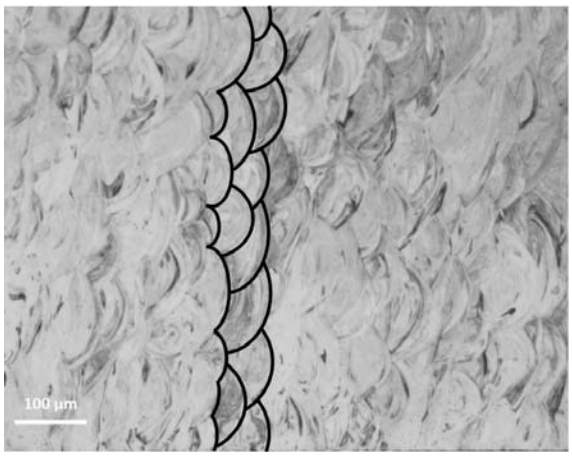

(a) Optical image of the macro structure perpendicular to the build plane

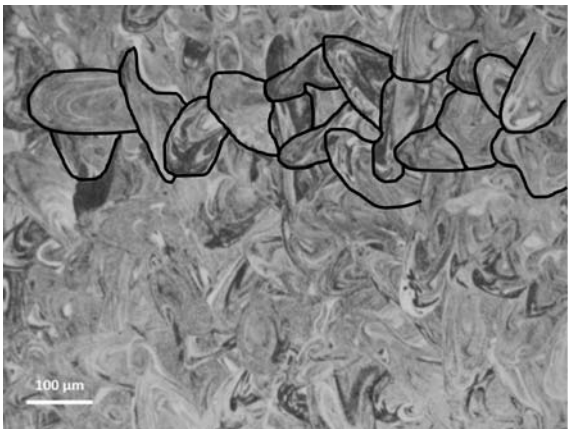

(b) Optical image of the macro structure in the build plane

Figure 4.25. Optical image of the macro structure in the build plane

	Size (um)	Standard Deviation (um)
Melt Pool Depth	48.4923	1.6995
Melt Pool Width	62.2542	1.672

Table 4.13. Melt pool dimensions results

4.3.2 Energy Dispersive X-ray Spectroscopy

EDS testing is important to determine the composition of the material. There is some inherent risk in the use of AM with regards to the composition of the material. The machines used to print AM parts are designed to use a variety of powder, and when switching from production of one material to another there is a risk that the machine isn't cleaned properly and left over powder contaminates the new part. There is also a risk that recycled old powder can contaminate new new powder. Previous work by Dempsey [17] showed the potential of variation in the composition of builds that were all supposed to be the same material. This requires the use of EDS to verify the composition of the material. Because the accuracy of EDS with elements that have a smaller atomic number then oxygen [15] is poor, the Carbon results are excluded. The results of the EDS testing on the materials used in this test effort are

shown in figure 4.14.

Element	AISI Weight Percent	Material Composition (%)	SHPB Tension (%)
C	0.07 max	N/A	N/A
Mn	1.00 max	0.31	0.54
Si	1.00 max	0.61	0.76
Cr	14.00-15.50	12.47	14.29
Ni	3.50-5.50	5.7	4.16
Mo	0.50 max	0	0
Nb	0.15-0.45	0.38	0.37
Cu	2.50-4.50	2.96	3.45
Fe	71.90-77.70 Balance	74.49	75.12

Table 4.14. EDS results results

The results of the EDS show that the SHPB tension material is within the specifications of AISI. The new build used for all of this testing has a slightly lower amount of Chromium and slightly high amount of Nickel. The reduction in chromium will have a small impact on the corrosion resistance of the steel but should not effect the overall strength of material properties. The increased amount of Nickel should have very little effect on the material as it is added to increase corrosion resistance.

4.3.3 Energy Dispersive X-ray Spectroscopy

EBSD micrographs were taken of the specimens to analyze the effect of the microstructure on the mechanical properties. The alloying elements in 15-5PH were selected to form a martensitic structure upon cooling so the anticipated crystal structure is martensite[20]. The results from the EBSD shown in figure 4.26 shows that the microstructure is primarily martensite with a small amount of austenite. Wrought 15-5PH stainless steel material is entirely martensite with no retained or reverted austenite. Recent research into the microstructure of 15-5PH created through the DMLS process results has shown a small amount of retained/reverted austenite[8].

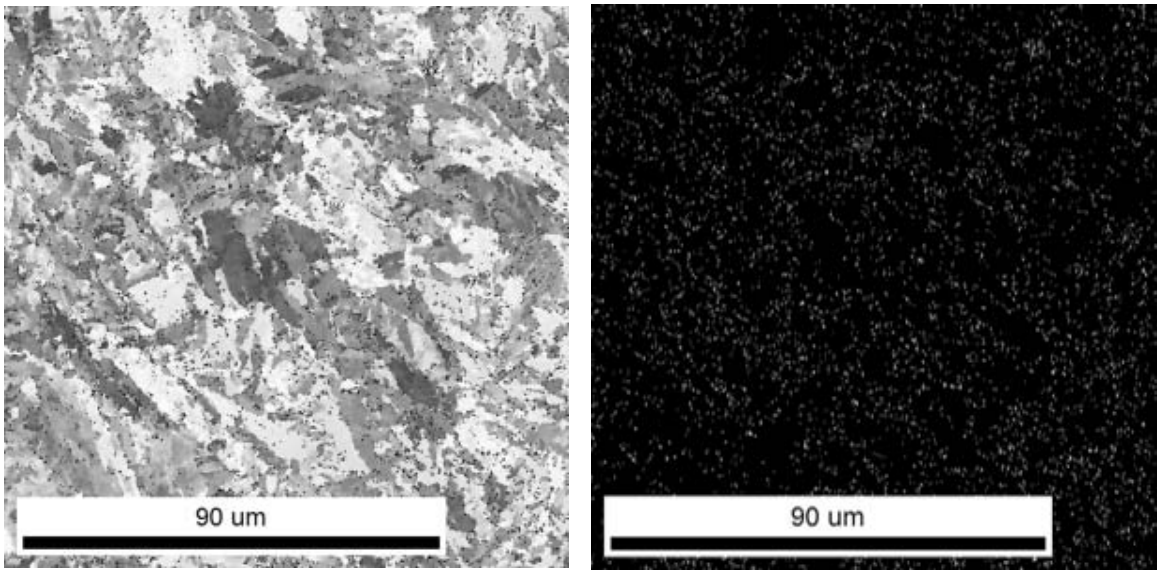

(a) Martensitic microstructure **(b) Austenitic microstructure**

Figure 4.26. Microstructure in the build plane of an untested H900 horizontal specimen

The effect of build orientation was analyzed by taking micrographs both in the plane of the build and against the plane of the build. Figure 4.27 shows a comparison of the out of plane microstructure of a horizontal specimen to the in plane microstructure of a vertical specimen after the H900 heat treatment. This shows how the microstructure is different between in plane and out of plane directions and how that may affect the mechanical properties resulting in anisotropy. Figure 4.28 shows the in plane microstructure of an untested H900 vertical specimen, quasi-static compression tested H900 vertical specimen and quasi-static compression tested Condition A vertical specimen. These micrographs show that the microstructure perpendicular to the build plane has a larger amount of grain high angle grain mis-orientations. The high angle grain mis-orientations correlate to an increase in material strength.

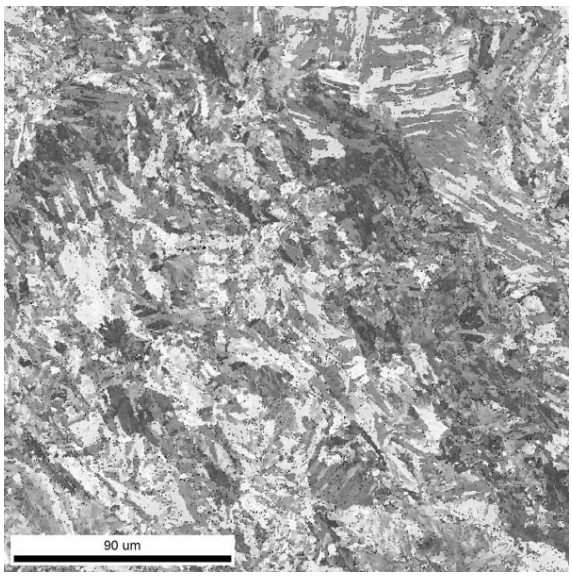

(a) Microstructure perpendicular to the build plane

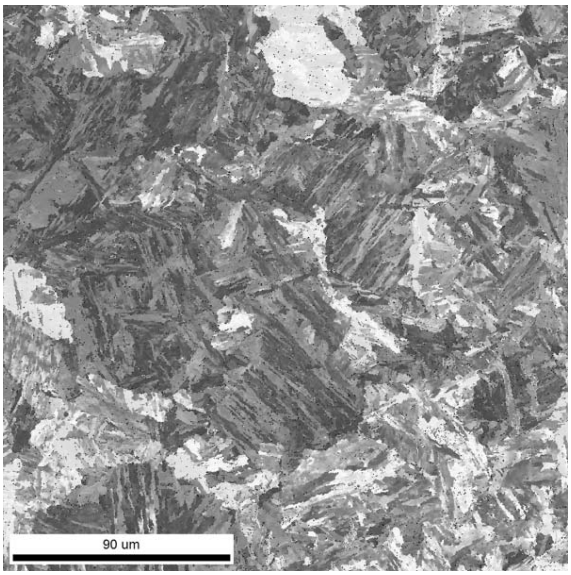

(b) Austenitic microstructure

Figure 4.27. Comparison of the microstructure in the build plane and perpendicular to the build plane

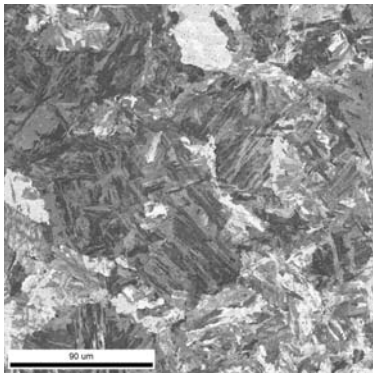

(a) H900 untested

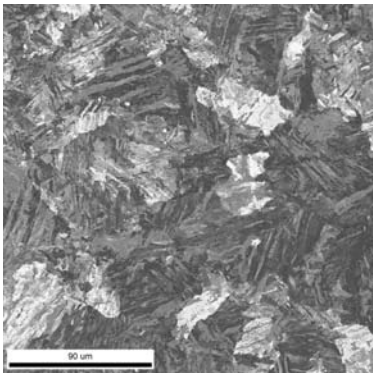

(b) H900 quasi static compression tested

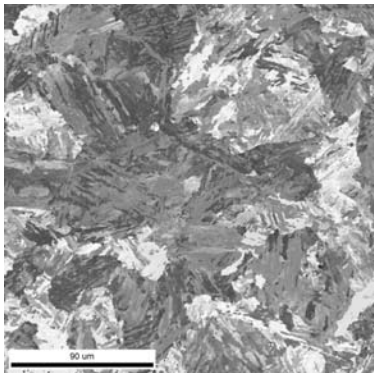

(c) Condition A untested

Figure 4.28. Comparison of the microstructure in the build plane across heat treatments

Figure 4.29 shows the out of plane microstructure of an untested Condition A horizontal specimen, untested H900 horizontal specimen and quasi-static compression tested Condition A horizontal specimen. These figures show no significant change in the microstructure by the heat treatment, or the quasi-static compression testing. The heat treatment mechanism for this precipitation hardening steel is through the formation of Cu precipitates inside the lath structure. These Cu precipitation that form are approximately 5nm in diameter so it is not possible to see their formation unless using a transmission electron microscope[21].

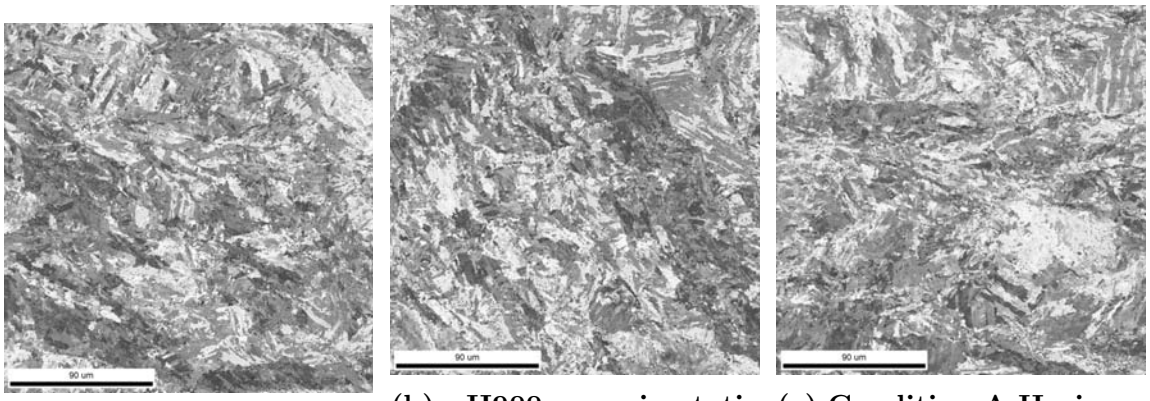

(a) Condition A untested **(b) H900 quasi static compression tested** **(c) Condition A Horizontal untested**

Figure 4.29. Comparison of the microstructure in the build plane across heat treatments

4.3.4 Analysis of the Mechanical Testing

4.3.4.1 Analysis of the Mechanical Testing

The results of the mechanical testing showed several clear trends in the data. The first trend is the effect of the build orientation on the mechanical properties of the material. The following tables compares the vertical orientation to the horizontal and show the increase, or decrease of the vertical orientation over the horizontal. Table 4.15 shows how the build orientation effects the yield stress for the compression testing. The anisotropy is present at the quasi-static testing and only increases with

heat treatment and increasing strain rate. Table 4.16 shows how the build orientation effects the UTS and FS for the tension tests. The tension testing also shows anisotropy between orientations. The UTS shows a relatively small anisotropy of around 3% difference across the heat treatments and strain rates. The H900 quasi-static point shows the largest amount of anisotropy in the UTS. The FS shows a very significant impact of the build orientation. Across all the test points and heat treatments the horizontal orientation has a much higher failure strain. This shows that the horizontal orientation is more ductile and tougher than the vertical specimens.

Compression test	Condition A	H900
QS compression YS (%)	4.504	9.976
Low rate compression YS (%)	6.408	13.808
High rate compression YS (%)	8.062	16.559

Table 4.15. The effect of the build orientation across the compression test points

Tension test	Condition A	As Built	H1025	H900
QS Tension UTS (%)	1.996	N/A	N/A	10.408
QS Tension FS (%)	-22.812	N/A	N/A	-26.478
LR Tension UTS (%)	N/A	2.656	3.275	2.229
LR Tension FS (%)	N/A	-25.132	-25.918	-32.432
HR Tension UTS (%)	N/A	4.773	4.343	2.668
HR Tension FS (%)	N/A	-29.338	-34.240	-25.935

Table 4.16. The effect of the build orientation across the tension test points

The second trend is the effect of the heat treatment on the mechanical properties of the material. The wrought material exhibits a 44% increase in the YS. The following tables show the increase in YS and UTS for the given orientation, heat treatment and test condition. Table 4.17 shows how the heat treatment effects the yield stress for the compression testing. The table shows that the vertical samples react more strongly to the heat treatment, but neither orientation increases as strongly as the wrought material.

In tension testing the wrought material also shows an increase in the UTS of 30%

for the H900 heat treatment and 8% for the H1025 heat treatment. The increase in the FS is 20% for the H900 heat treatment and 45% for the H1025 heat treatment. Table 4.18 shows how the heat treatment effects the UTS and FS for the tension testing. One important note that was discussed earlier is the significant increase in the FS of the AM material. The FS of all the AM material is higher than the wrought material. The only heat treatment that experiences an increase in FS is the H900 horizontal, it also experiences a significant increase in UTS. All other heat treatments show a reduction in FS along with and increase in UTS. The impact of the heat treatment is very comparable for the low rate and high rate test conditions.

Compression Test	H900 Horizontal	H900 Vertical
QS Compression YS (%)	30.378	32.625
LR Compression YS (%)	26.567	35.370
HR Compression YS (%)	18.168	27.460

Table 4.17. The effect of the heat treatment across the compression test points

Tension Test	H900 Horizontal	H900 Vertical	H1025 Horizontal	H1025 Vertical
QS Tension UTS (%)	35.720	45.276	N/A	N/A
QS Tension FS (%)	23.170	-17.231	N/A	N/A
LR Tension UTS (%)	23.266	24.008	11.869	11.404
LR Tension FS (%)	-18.629	-19.484	-8.963	-17.840
HR Tension UTS (%)	22.566	22.063	13.454	11.175
HR Tension FS (%)	-21.109	-26.582	-23.435	-19.747

Table 4.18. The effect of the build orientation across the compression test points

4.3.4.2 Johnson Cook Model

The Johnson Cook equation one of the most widely used material models for calculating the the stress of a material undergoing deformation in the plastic regime. The model takes into account the stress-strain relationship under plastic deformation, the stress-strain rate relationship, and the stress-temperature relationship. The Johnson cook equation is shown in equation 4.1 where T_m is the melting temperature and T_0 is the room temperature[22].

$$\sigma_{=}[A + B\epsilon^n][1 + Cln(\frac{\dot{\epsilon}}{\dot{\epsilon}_0})][1 - (\frac{T - T_0}{T_m - T_0})^m] \tag{4.1}$$

The five constants for the Johnson Cook model are: A, B, C, n and m. For these constants A represents the yield stress, B the strain factor, C the strain rate sensitivity coefficient, n the the strain hardening exponent, m the temperature exponent and $\dot{\epsilon}/\dot{\epsilon_0}$ the plastic strain rate reference. The results of the Johnson Cook coefficients calculated from this testing are shown in table 4.19. For the compression results the value for A was specified as the yield stress calculated from the quasi-static testing, and a least squared method was used to calculate the other parameters. The tests for this effort were all accomplished at room temperature so T-T_0 is zero eliminating the effect of temperature. Plots of the compression Johnson Cook model are shown in figure 4.30 with the tension results shown in figure 4.31. A comparison of both the tension and compression results are shown in figure 4.34. Figure 4.32 and 4.33 show a plot of the experimental data compared to the Johnson Cook models that were calculated.

	A	B	n	C	m
Tension H900 Horizontal	184633	150404	0.3700	0.0197	0.6300
Tension H900 Vertical	215091	273252	0.8370	0.0220	0.6300
Compression H900 Horizontal	182748	162007	0.4433	0.0036	0.6300
Compression H900 Vertical	200878	145908	0.4273	0.0063	0.6300

Table 4.19. The Johnson Cook Coefficients

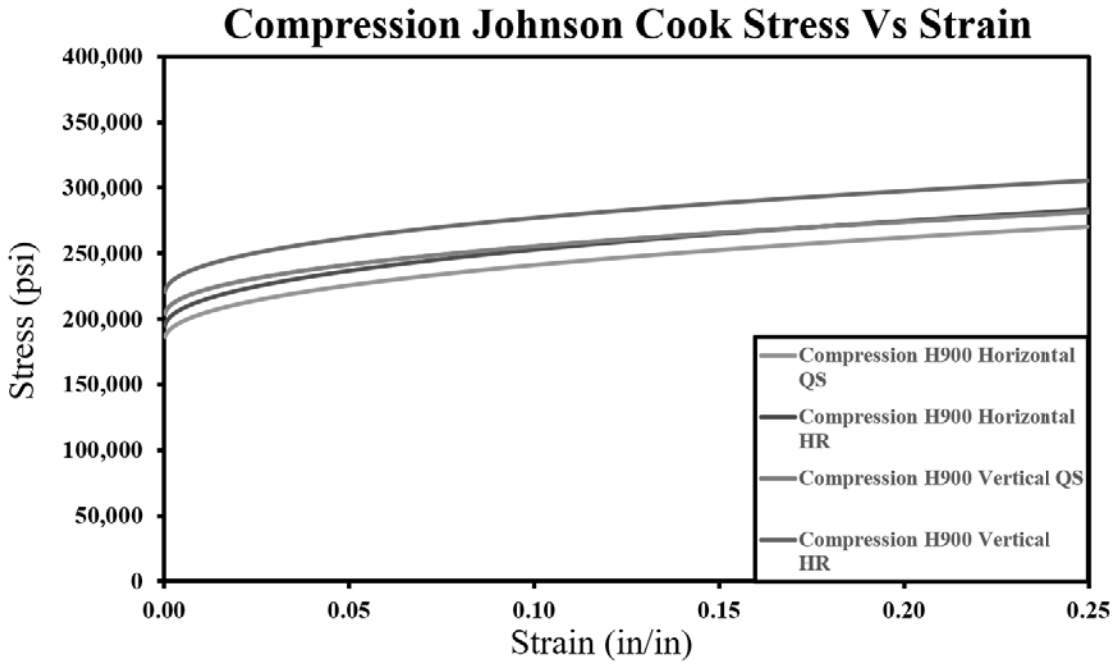

Figure 4.30. Johnson Cook model for the plastic compression response of the H900 heat treatment for both build orientations

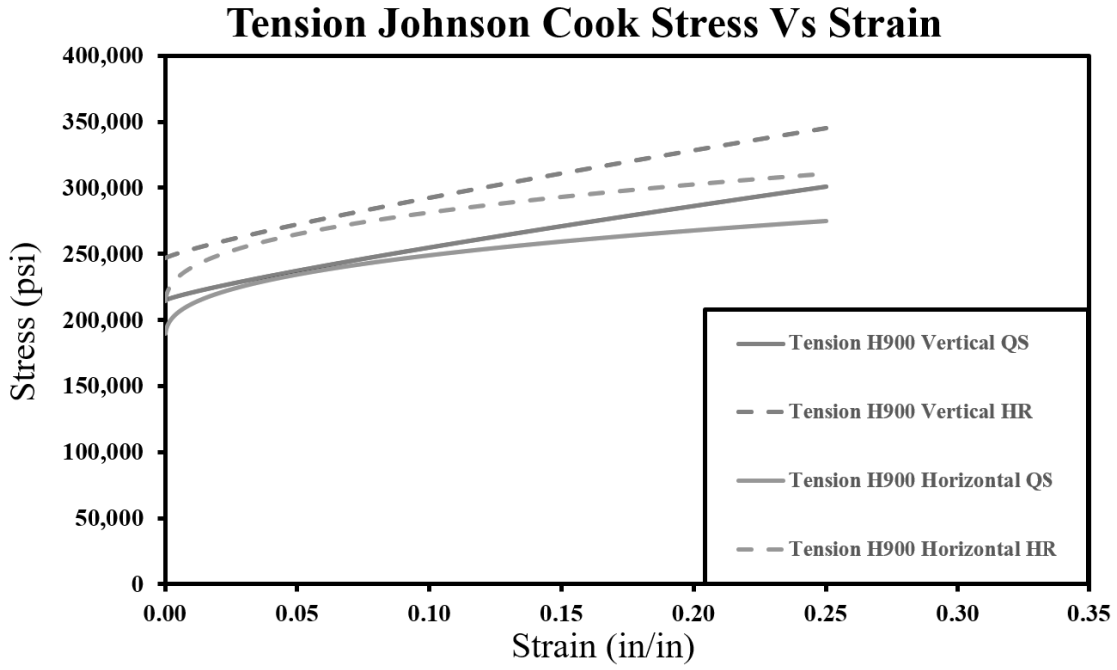

Figure 4.31. Johnson Cook model for the plastic tension response of the H900 heat treatment for both build orientations

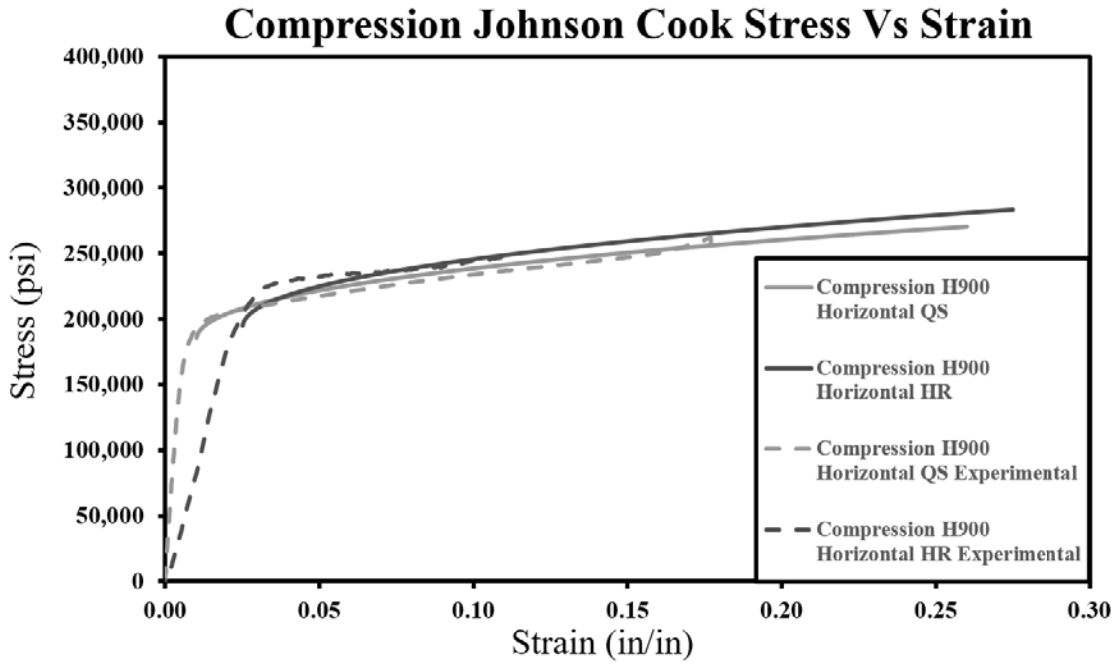

Figure 4.32. Johnson Cook model for the plastic tension response of the H900 heat treatment for both build orientations

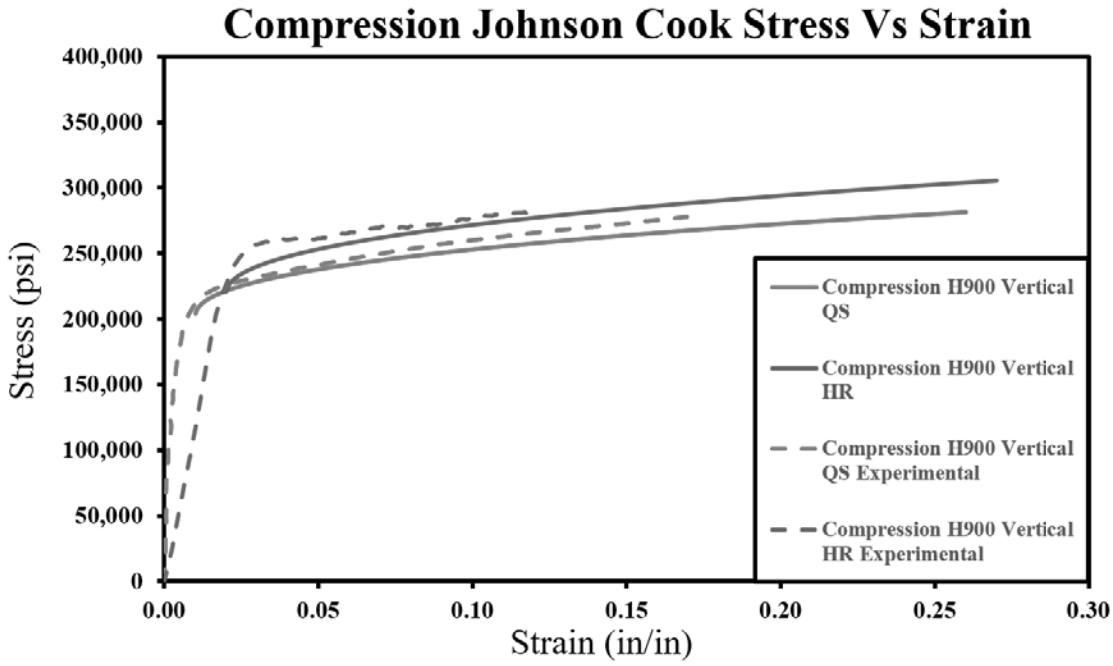

Figure 4.33. Johnson Cook model for the plastic tension response of the H900 heat treatment for both build orientations

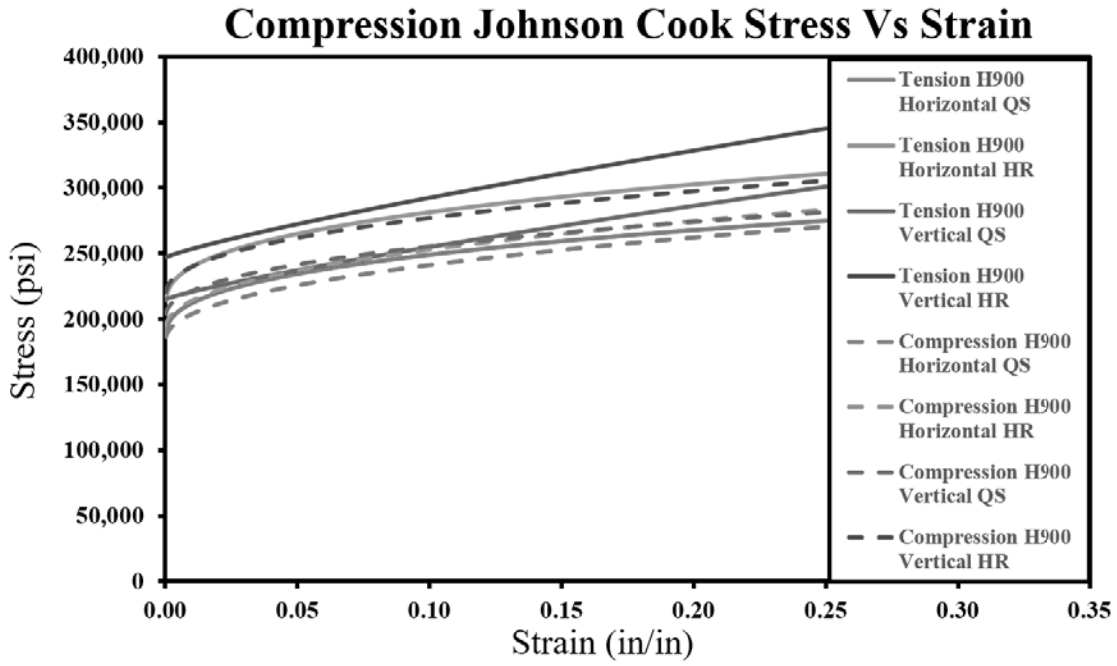

Figure 4.34. Johnson Cook model for the plastic tension and compression response of the H900 heat treatment for both build orientations

4.3.5 Analysis of the Microstructural Results

The microstructure of steel is very important in determining the strength and behavior of the material. A comparison between the microstructure revealed in the EBSD and the macro structure revealed by the optical microscopy shows a correlation between the formation of the martensitic structure and the macro structure. Figure 4.35 shows a comparison of the EBSD in the build plane to the optical macro structure in the build plane. This shows how the martensite forms within the melt pool and the growth is limited to the weld pool edges. This shows the formation of large martenisitic packets that are broken into large blocks within the microstructure. Figure 4.36 shows the comparison of the EBSD perpendicular to the build plane to the optical macro structure perpendicular to the build plane. This figure shows how the martensite forms within the melt pool and is stopped at the edges of the weld pool. Because the width of the weld pool is larger than the depth of the weld pool

this allows for a larger formation of martensite packets. This correlation between the melt pool dimensions and the formation of the martensite within the melt pool show how the manufacturing method can effect the microstructure.

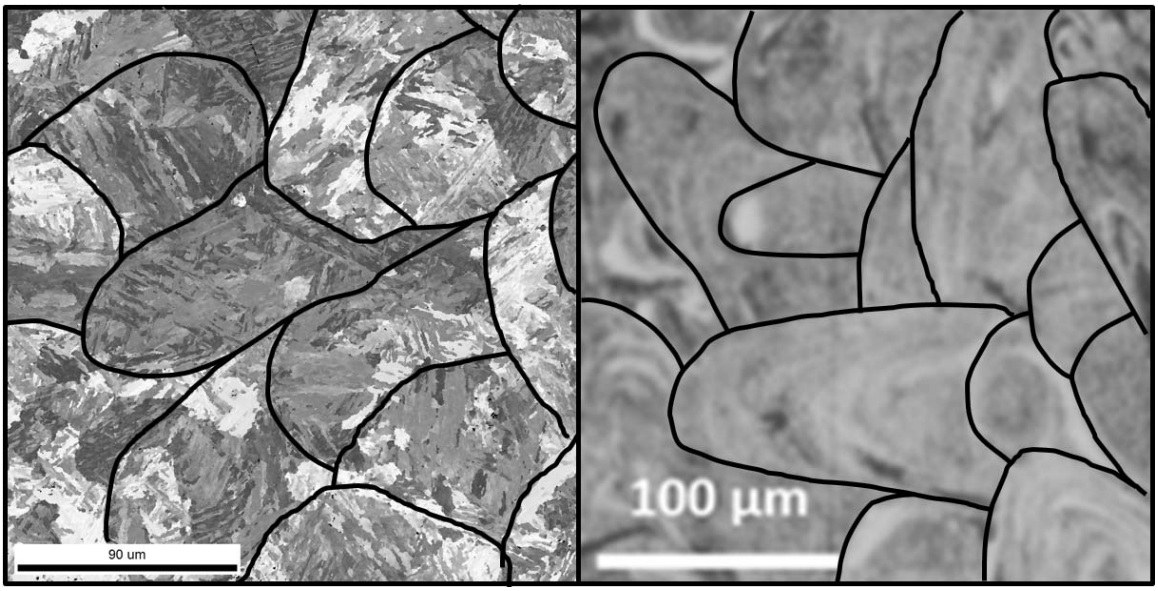

Figure 4.35. Comparison of EBSD and Optical micrograph in the build plane

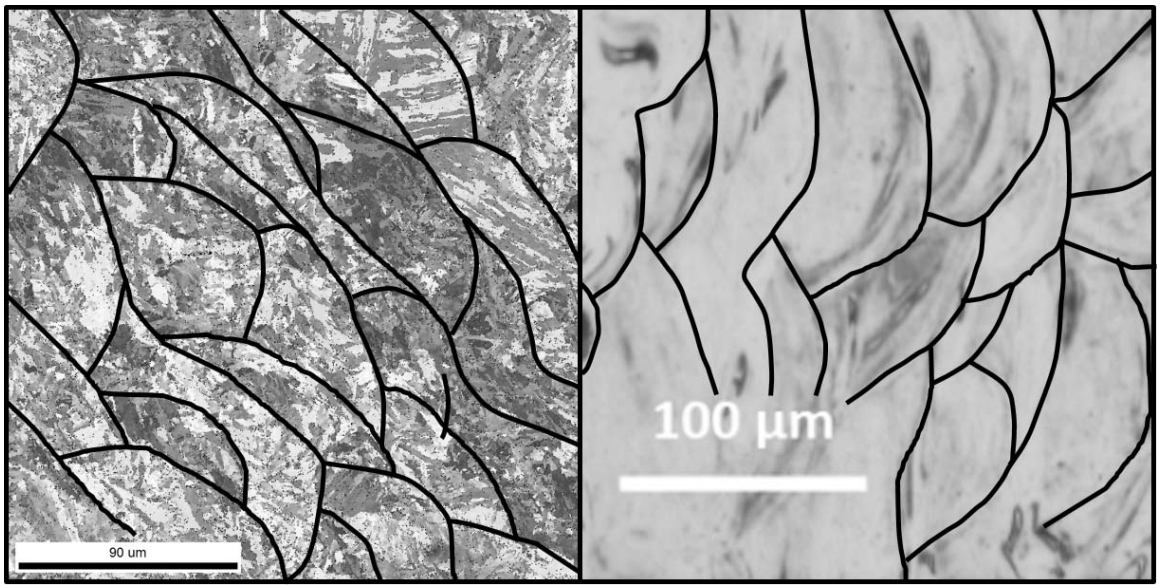

Figure 4.36. Comparison of EBSD and Optical micrograph perpendicular to the build plane

V. Conclusions and Recommendations

Chapter five is the final chapter and will discuss the conclusions that have been drawn from the results of the tests and future work that could be done on this subject. Chapter five will be splits into 2 sections. The first section will review the conclusions that have resulted from the work done. The objective of this research was to establish the mechanical properties of AM 15-5PH stainless steel, and the results of the conducted tests will establish them. The three variables that were analyzed in this effort were the build orientation, heat treatment and strain rate. In order to characterize the effect these three variables have on the material properties 20 quasi-static compression tests, 16 quasi-static tension tests, 24 SHPB compression test and 23 SHPB tension tests were conducted. The samples for the quasi-static and SHPB compression tests were all manufactured as a part of a single build. The SHPB tension results were from a separate build that met the required standards for AISI 15-5 PH material. A single manufacture run was desired to eliminate the build to build variations that may effect the material properties. Build orientation was analyzed by testing samples with opposing orientations, vertical and horizontal orientations. The effect of the DMLS build process on the Heat treatment was analyzed by looking at Condition A samples, and samples undergoing the H900 heat treatment. The effect of strain rate was analyzed by comparing the results of quasi-static tests with a strain rate of 10^{-3} s^{-1} to the results of SHPB test conducted at 500 s^{-1} and 800 s^{-1}.

The second section will discuss recommendations for future work in this area. This sections will review some of the problems that were discovered during this testing and potential areas of research that could be conducted. This sections will also review further analysis that could be conducted in other areas that could help analyze how the AM process effects the mechanical properties. The proposed work will include recommendations to further understand both the mechanical properties of the

material as well as the microstructural properties and how the two interact.

5.1 Conclusions

The results of this effort have accomplished the objective to establish the mechanical properties of AM 15-5 PH stainless steel, and the effects that the DMLS process has on the material. The data collected from the quasi-static testing allowed a direct comparison of the AM material's mechanical properties to the wrought material's. The results from the two different heat treatments provided two comparison points with the wrought material as well as providing additional information on how the AM process potentially effects the hardening of precipitation hardening materials. Testing at dynamic strain rates enabled the ability to characterize the effect of strain rate on the mechanical properties of AM materials. The microstructure was also examined in order to characterize the effect the DMLS process has on the microstructure and how it may effect the mechanical properties. The microstructural analysis also provided insight into the effects seen in the mechanical properties of the material.

5.1.1 Material Performance

The results of the quasi-static testing showed comparable results to the wrought material. The tension tests revealed the Condition A YS was about 6.4% lower than the wrought material for both the vertical and horizontal build orientations. The H900 horizontal build orientation was 11% lower than the wrought material with the vertical build orientation only 5% lower. The results of the UTS was much closer to the wrought material. The UTS was only about 1% different for both the Condition A orientations but it was 8% lower for the H900 horizontal orientation. The modulus of elasticity for both the H900 orientations is within 1% of the wrought material. The wrought material does not give a modulus of elasticity for the Condition A material

but the results show it to be 35% lower than the modulus for the H900 heat treatment. This value makes is appropriate because Condition A is designed to be a softer more machinable condition of the material. T

5.1.2 Build Orientation

The build orientation appeared to have a significant impact on the mechanical properties. Across almost every test point the vertical build orientation showed YS and higher UTS. The effect of the build orientation was very visible across the compression testing. The Condition A vertical YS was 4.5% stronger for the quasi-static tests, 6.4% stronger for the low rate compression tests and 8% stronger for the high rate compression tests than the horizontal orientation. The tension testing did not show much difference in the build orientation but did show a 7% increase in the YS for the H900. The effect was difficult to quantitatively measure for the tension SHPB tests. It was determined that the specimen was not in stress equilibrium during the elastic portion of these tests which resulted in inaccurate measurements for the YS. A general trend from looking at the graphs shows the vertical specimens show increased stress over the horizontal specimens. The UTS also shows the trend of increased strength for the vertical specimens over the horizontal. Quasi-static testing show the vertical Condition A specimens are 7% higher and the H900 specimens 10.4% higher. The vertical As Built specimens show a 2.7% increase with the vertical H1025 showing a 2.3% increase and the vertical H900 exhibiting a 2.2% increase at the low strain rate conditions. At the high strain rate test point the vertical orientation samples show a 4.8% increase for the As Built condition, a 4.3% increase for the H1025 condition and a 2.7% increase for the H900 condition. The effect of the build orientation in compression increases with both heat treatment and strain rate, showing that at higher strengths the anisotropy increases, with the opposite effect for tension. In tension

the anisotropy is highest for the quasi static conditions but decreases with increasing strain rate.

The build orientation anisotropy can be seen be looking at the microstructure. The vertical specimens are being tested with the forces that act perpendicular to the build plane. The horizontal specimens are being tested with the forces acting in the build plane. The microstructure shows a significant difference between the build planes. The microstructure that is perpendicular to the build plane is limited by the depth of the melt pool which is smaller than the width. This limits size of the packets that can from, resulting in smaller packets, and blocks. There is also a higher formation of mis-oriented grains in the perpendicular to the build plane. Because the heat treatment acts by forming precipitates in the steel, if they preferential form at lath boundaries the vertical specimens would react more to the heat treatment.The testing and the microstructure show that 15-5 PH material exhibits a small amount of anisotropy that should be accounted for when using this material.

5.1.3 Heat Treatment

The H900 heat treatment of traditional wrought material increases the YS by 43.6% and the UTS by 29.8%. The H1025 heat treatment increases the YS by 8.1% and the UTS by 22.1%. The heat treatment process for 15-5PH increases the strength of the material by forming copper precipitates. These copper precipitates are too small to be detected by the EBSD techniques so it has to be assessed by the YS and UTS. The quasi-static compression testing yielded very similar results to the wrought material. The H900 samples showed about a 30% increase in YS for the quasi-static testing that was reduced for the low strain rate testing and reduced even further for the high strain rate testing. For the quasi-static tension testing we see a 35.7% increase for the horizontal specimen, and a 45.3% increase for the vertical specimen.

The UTS is increased by 20.4% for the horizontal samples and 30.3% for the vertical samples. This results show that the DMLS material reacts to the heat treatment the same as wrought material. The vertical build orientation continues to show an increased strength over the horizontal orientation. This anisotropy between the build orientations is strongest in compression. In tension the anisotropy reduces as the strain rate increases. The DMLS material reacts to the heat treatment as expected, however it does show anisotropic behavior between the vertical and horizontal builds.

5.1.4 Material Composition

The material composition of steel is extremely important to achieve the desired strength. The build used for the quasi-static and SHPB compression testing was slightly outside the AISI specifications for 15-5 PH. The alloying elements that did not meet the AISI standards are added for corrosion resistance and so have minimal impact on the strength of the material. The build used for the SHPB tension testing met the AISI standards. The work by Dempsey[17] showed how much variability can occur between builds that are all supposed to be of the same material. Care should be taken when purchasing parts via AM to verify the composition of the material. The ability of the new process to recycle the powder between builds can result in powder contamination. The build can also be contaminated if the machine is not properly cleaned between builds.

5.2 Future Work

5.2.1 Material Performance

To fully characterize the material a full investigation of the Johnson-Cook parameters should be conducted. The Johnson-Cook equation characterizes the behavior of the material over a large variety of strain rates and varying temperature. Future

work could explore the effect of the multiple strain rates between the quasi- static value 10^{-3} s^{-1} and extremely high strain rates on the order of 10^{4} s^{-1}. These tests should be accomplished using a single build to limit the effect of build variability on the test results. Testing should also be done at varying temperatures from room temperature to 600 °F. Further analysis of the strain rate and the temperature effect on the material properties would produce the full Johnson-Cook equation. The full Johnson-Cook equation could be used in finite element modeling software to increase the accuracy of their models for AM 15-5 PH materials.

5.2.2 Build Parameters

This research effort used the recommended settings by the manufacturer for this material. These settings may change between manufacturers and an understanding of how these settings effect the strength of the material should be accomplished. One of the key areas of focus for DMLS materials is how the change in build parameters can effect the material. Incorrect parameters can result in keyhole defects within the material, or a failure to fully sinter the powder resulting in material that is not fully dense. These defects can result from either too high or to low laser power, laser spot size, laser pulse frequency, laser pulse duration, scan speed and scan spacing. Establishing build parameters for different manufacturers and builds would reduce the variability.

The powder used can also have an impact on the build. Using recycled powder increases the risk of powder contamination. For recycled powder there is a risk of cross contamination between builds of different materials and the risk of oxidation occurring in old recycled powder. If oxidized powder is in the middle of a build it can create internal defects. Powder made by different manufactures may also have different densities, particle size and a large variation on particle size, all of which will

affect the final product. Future research can analyze how the use of powders from different manufactures affects the strength of material.

5.2.3 Microstructure

One of the major findings in this research was that of the retained austenite in the microstructure. Retained austenite is softer and more ductile than martensite and reduces the YS and UTS. Further research should be conducted to discover why the retained austenite occurs in the DMLS produced material. One area of analysis is the Nitrogen content of the material. Nitrogen is known as an austenite promoter and can effect the transition from martensite to austenite. During the production of the powder in a Nitrogen gas environment and the use of Nitrogen as the atmosphere for during the AM process there is a risk of increasing the Nitrogen content of the alloy. Another area for research is reducing the quench temperature after annealing the material. The M_f temperature is approximately room temperature depending on the composition. Further cooling of the steel beyond room temperature could ensure the fully martensitic microstructure despite any minor variation in the composition.

5.2.4 Machine Compliance

During the quasi-static testing there was significant error in the calculation of the strain by the testing machine. The effect of machine compliance is not very well defined on the strain. Further investigation into how the machine compliance affects the result of the strain could be examined. An analysis on the effects of the specimen size and stiffness on the measured strain could help the characterize the effects of compliance and how to avoid it impacting the test.

Bibliography

[1] D. W. R. Ian Gibson and B. Stucker, *Additive Manufacturing Technologies*, 1st ed. New York, NY: Springer, 2010.

[2] A. S. for Metals, *Volume 1 Properties and Selection of Iron*. Materials Park, OH: American Society for Metals International, 2005.

[3] R. E. Smallman and A. Ngan, *Physical Metallurgy and Advanced Materials, Seventh Edition.*, 7th ed. Burlington, MA: Butterworth-Heinemann, 2007.

[4] J. Verhoeven, *Steel Metallurgy for the Non-Metallurgist*. Materials Park, OH: American Society for Metals International, 2007.

[5] G. Totten and M. Howes, *Steel Heat Treatment Handbook*. New York, NY: Marcel Dekker, Inc., 1997.

[6] T. Morsdorf and Raabe, "3d structural and atomic-scale analysis of lath martensite: Effect of the transformation sequence," *Acta Materialia*, vol. 95, pp. 1366–377, 2015.

[7] H. H. Bajguirani, "The effect of ageing upon the microstructure and mechanical properties of type 15-5ph stainless steel," *Materials Science and Engineering*, vol. 338, pp. 142–159, 2002.

[8] K. M. Coffey, "Microstructure and chemistry evaluation of direct metal laser sintered 15-5ph stainless steel," Master's thesis, University of Central Florida, Orlando, Florida, 2014.

[9] A. S. for Metals, *Stainless Steels*. Materials Park, OH: American Society for Metals International, 1994.

[10] S. Kalpakjian and S. R. Schmid, *Manufacturing Engineering and Technology*, 3rd ed. Reading, MA: Addison-Wesley Publishing Company, 1995.

[11] D. Askeland and P. Phule, *The Science and Engineering of Materials*, 5th ed. Toronto, Ontario: Nelson, 2006.

[12] J. O. M. Sutton and H. Schreier, *Image Correlation for Shape, Motion and Deformation Measurements*. New York, NY: Nelson, 2009.

[13] W. W. Chen and B. Song, *Split Hopkinson (Kolsky) Bar: Design, Testing and Applications*. New York, NY: Springer, 2011.

[14] J. Heath and N. Taylor, *Essential Knowledge Briefings: Energy Dispersive Spectroscopy.*, 2nd ed. Chichester, West Sussex: John Wiley and Sons Ltd, 2015.

[15] *ASTM E1019-11 Standard Test Methods for Determination of Carbon, Sulfur, Nitrogen and Oxygen in Steel, Iron, Nickel and Cobalt Alloys by Various Combustion and Fusion Techniques*, American Society for Testing Materials, 2011.

[16] O. Instruments, *EBSD Explained from Data Acquisition to Advanced Analysis*. Oxfordshire, England: Oxford Instruments plc, 2015.

[17] A. A. Dempsey, "Effects of additive manufacturing methods on the dynamic properties of 15-5ph stainless steel," Master's thesis, Air Force Institute of Technology, Wright Patterson AFB, Ohio, 2015.

[18] G. Slotwinski and Hebenstreit2, "Porosity measurements and analysis for metal additive manufacturing process control," *Journal of Research of the National Institute of Standards and Technology*, vol. 119, 2014).

[19] Instron, *7 Tips for Material Testing*, Norwood, MA, 2006.

[20] A. S. for Metals, *Volume 9 Metallography and Microstructures*, 1st ed. Materials Park, OH: American Society for Metals International, 1992.

[21] D. Couturier, De Geuser and Deschamps, "Evolution of the microstructure of a 15-5ph martensitic stainless steel during precipitation hardening heat treatment," *Materials and Design*, vol. 107, p. 416425, 2016.

[22] Cook and Johnson, "A constitutive model and data for metals subjected to large strains, high temperatures," *Proceedings of the seventh International Symposium on Ballistic*, vol. 1, pp. 541–547, 1983.

REPORT DOCUMENTATION PAGE

Form Approved
OMB No. 0704-0188

The public reporting burden for this collection of information is estimated to average 1 hour per response, including the time for reviewing instructions, searching existing data sources, gathering and maintaining the data needed, and completing and reviewing the collection of information. Send comments regarding this burden estimate or any other aspect of this collection of information, including suggestions for reducing the burden, to Department of Defense, Washington Headquarters Services, Directorate for Information Operations and Reports (0704-0188), 1215 Jefferson Davis Highway, Suite 1204, Arlington, VA 22202-4302. Respondents should be aware that notwithstanding any other provision of law, no person shall be subject to any penalty for failing to comply with a collection of information if it does not display a currently valid OMB control number.
PLEASE DO NOT RETURN YOUR FORM TO THE ABOVE ADDRESS.

1. REPORT DATE *(DD-MM-YYYY)*	2. REPORT TYPE	3. DATES COVERED *(From - To)*
23-3-2017	Master's Thesis	August 2016 - March 2017

4. TITLE AND SUBTITLE
Mechanical Properties of Additively Manufactured Stainless Steel

5a. CONTRACT NUMBER

5b. GRANT NUMBER

5c. PROGRAM ELEMENT NUMBER

6. AUTHOR(S)
Lum, Eric W, Capt

5d. PROJECT NUMBER
JON 17Y331

5e. TASK NUMBER

5f. WORK UNIT NUMBER

7. PERFORMING ORGANIZATION NAME(S) AND ADDRESS(ES)
Air Force Institute of Technology
Graduate School of Engineering and Management (AFIT/EN)
2950 Hobson Way
Wright-Patterson AFB OH 45433-7765

8. PERFORMING ORGANIZATION REPORT NUMBER
AFIT-ENY-MS-17-M-273

9. SPONSORING/MONITORING AGENCY NAME(S) AND ADDRESS(ES)
Air Force Research Lab RWM
101 West Eglin Blvd
Attn: Donald Littrell
Eglin AFB FL 32542
DSN 872-6802, COMM 850-882-6802

10. SPONSOR/MONITOR'S ACRONYM(S)
AFRL

11. SPONSOR/MONITOR'S REPORT NUMBER(S)

12. DISTRIBUTION/AVAILABILITY STATEMENT
DISTRIBUTION STATEMENT A:
APPROVED FOR PUBLIC RELEASE; DISTRIBUTION UNLIMITED.

13. SUPPLEMENTARY NOTES

14. ABSTRACT

This research analyzes the effects of the Additive Manufacturing process, Direct Metal Laser Sintering technique, on the mechanical properties of 15-5 PH stainless steel. In order to understand how the material properties are effected by the AM process this research will analyze the effect of build orientation, heat treatment and strain rate on the material. The conducted research used quasi-static and Split Hopkinson Pressure Bar testing to evaluate the mechanical properties of 15-5PH stainless steel. This on-going research will extend the previous analysis of tension loading at high strain rates analysis to compression loading at high strain rates. Electron backscatter diffraction (EBSD) will be used to analyze the micro-structure of specimens to characterize the affect that the DMLS process has on the microstructure. The results of the compression testing will be compared to the results from the tension testing to compare the mechanical response to the two different load types.

15. SUBJECT TERMS
^Additive Manufacturing, Stainless Steel, 15-5PH, Split Hopkinson Pressure Bar

16. SECURITY CLASSIFICATION OF:			17. LIMITATION OF ABSTRACT	18. NUMBER OF PAGES	19a. NAME OF RESPONSIBLE PERSON
a. REPORT	b. ABSTRACT	c. THIS PAGE			Dr. Anthony Palazotto, AFIT/ENY
U	U	U	UU	111	19b. TELEPHONE NUMBER *(Include area code)* (937) 255-3636, x4599 anthony.palazotto@afit.ed

INSTRUCTIONS FOR COMPLETING SF 298

1. REPORT DATE. Full publication date, including day, month, if available. Must cite at least the year and be Year 2000 compliant, e.g. 30-06-1998; xx-06-1998; xx-xx-1998.

2. REPORT TYPE. State the type of report, such as final, technical, interim, memorandum, master's thesis, progress, quarterly, research, special, group study, etc.

3. DATES COVERED. Indicate the time during which the work was performed and the report was written, e.g., Jun 1997 - Jun 1998; 1-10 Jun 1996; May - Nov 1998; Nov 1998.

4. TITLE. Enter title and subtitle with volume number and part number, if applicable. On classified documents, enter the title classification in parentheses.

5a. CONTRACT NUMBER. Enter all contract numbers as they appear in the report, e.g. F33615-86-C-5169.

5b. GRANT NUMBER. Enter all grant numbers as they appear in the report, e.g. AFOSR-82-1234.

5c. PROGRAM ELEMENT NUMBER. Enter all program element numbers as they appear in the report, e.g. 61101A.

5d. PROJECT NUMBER. Enter all project numbers as they appear in the report, e.g. 1F665702D1257; ILIR.

5e. TASK NUMBER. Enter all task numbers as they appear in the report, e.g. 05; RF0330201; T4112.

5f. WORK UNIT NUMBER. Enter all work unit numbers as they appear in the report, e.g. 001; AFAPL30480105.

6. AUTHOR(S). Enter name(s) of person(s) responsible for writing the report, performing the research, or credited with the content of the report. The form of entry is the last name, first name, middle initial, and additional qualifiers separated by commas, e.g. Smith, Richard, J, Jr.

7. PERFORMING ORGANIZATION NAME(S) AND ADDRESS(ES). Self-explanatory.

8. PERFORMING ORGANIZATION REPORT NUMBER. Enter all unique alphanumeric report numbers assigned by the performing organization, e.g. BRL-1234; AFWL-TR-85-4017-Vol-21-PT-2.

9. SPONSORING/MONITORING AGENCY NAME(S) AND ADDRESS(ES). Enter the name and address of the organization(s) financially responsible for and monitoring the work.

10. SPONSOR/MONITOR'S ACRONYM(S). Enter, if available, e.g. BRL, ARDEC, NADC.

11. SPONSOR/MONITOR'S REPORT NUMBER(S). Enter report number as assigned by the sponsoring/ monitoring agency, if available, e.g. BRL-TR-829; -215.

12. DISTRIBUTION/AVAILABILITY STATEMENT. Use agency-mandated availability statements to indicate the public availability or distribution limitations of the report. If additional limitations/ restrictions or special markings are indicated, follow agency authorization procedures, e.g. RD/FRD, PROPIN, ITAR, etc. Include copyright information.

13. SUPPLEMENTARY NOTES. Enter information not included elsewhere such as: prepared in cooperation with; translation of; report supersedes; old edition number, etc.

14. ABSTRACT. A brief (approximately 200 words) factual summary of the most significant information.

15. SUBJECT TERMS. Key words or phrases identifying major concepts in the report.

16. SECURITY CLASSIFICATION. Enter security classification in accordance with security classification regulations, e.g. U, C, S, etc. If this form contains classified information, stamp classification level on the top and bottom of this page.

17. LIMITATION OF ABSTRACT. This block must be completed to assign a distribution limitation to the abstract. Enter UU (Unclassified Unlimited) or SAR (Same as Report). An entry in this block is necessary if the abstract is to be limited.